East Engineering

Journal of Research

of the

National Bureau of Standards

OCTOBER 1953

VOLUME 51 NUMBER 4

U. S. DEPARTMENT OF COMMERCE
Sinclair Weeks, Secretary
NATIONAL BUREAU OF STANDARDS
A. V. Astin, Director

OCTOBER • 1953
VOLUME • 51
NUMBER • 4

JOURNAL OF RESEARCH

of the

NATIONAL BUREAU OF STANDARDS

PERIODICALS OF THE NATIONAL BUREAU OF STANDARDS

The National Bureau of Standards is engaged in fundamental and applied research in physics, chemistry, mathematics, and engineering. Projects are conducted in thirteen fields: electricity, optics and metrology, heat and power, atomic and radiation physics, chemistry, mechanics, organic and fibrous materials, metallurgy, mineral products, building technology, applied mathematics, electronics, and radio propagation. The Bureau has custody of the national standards of measurement and conducts research leading to the improvement of scientific and engineering standards and of techniques and methods of measurement. Testing methods and instruments are developed; physical constants and properties of materials are determined; and technical processes are investigated.

JOURNAL OF RESEARCH

Internationally known as a leading scientific periodical, the Journal prints research papers by authorities in the specialized fields of physics, mathematics, chemistry, and engineering. Complete details of the work are presented, including laboratory data, experimental procedures, and theoretical and mathematical analyses. Annual subscription: domestic, $5.00; foreign, $6.75.

TECHNICAL NEWS BULLETIN

Summaries of current research at the National Bureau of Standards are published each month in the Technical News Bulletin. The articles are brief, with emphasis on the results of research, chosen on the basis of their scientific or technologic importance. Lists of all Bureau publications during the preceding month are given, including Research Papers, Handbooks, Applied Mathematics Series, Building Materials and Structures Reports, and Circulars. Each issue contains 12 or more two-column pages; illustrated. Annual subscription: domestic, $1.00; foreign, $1.35.

BASIC RADIO PROPAGATION PREDICTIONS

The Predictions provide the information necessary for calculating the best frequencies for communication between any two points in the world at any time during the given month. The data are important to all users of long-range radio communications and navigation, including broadcasting, airline, steamship, and wireless services, as well as to investigators of radio propagation and the ionosphere. Each issue, covering a period of one month, is released three months in advance and consists of large pages, including pertinent charts, drawings, and tables. Annual subscription: domestic, $1.00; foreign, $1.25.

Order all publications from the Superintendent of Documents
U. S. Government Printing Office, Washington 25, D. C.

The printing of this publication has been approved by the Director of the Bureau of the Budget, May 18, 1953.

Journal of Research of the National Bureau of Standards Vol. 51, No. 4, October 1953 Research Paper 2446

Determination of Carbon 14 in the Terminal Positions of Sugars: Preparation of D-Arabinose-5-C^{14} From D-Fructose-1,6-C^{14} (1, 2)

Harriet L. Frush and Horace S. Isbell

Methods are described for the determination of carbon 14 in the terminal positions of reducing sugars. The sugar in alkaline solution is oxidized by means of molecular oxygen to the next lower aldonic acid, and the acid is separated in the form of a convenient derivative. The loss in radioactivity coincident with the removal of carbon 1 is a measure of the activity located at this carbon. The activity of the carbon at the nonreducing end of the molecule is determined by periodate oxidation of the aldonic acid, followed by formation and radioactivity assay of the dimedone compound of the resulting formaldehyde.

The method was applied to the labeled D-fructose prepared from D-mannitol-1-C^{14} by the action of *Acetobacter suboxidans*, and the D-arabonic acid formed from the D-fructose was isolated as potassium D-arabonate. It was found that all of the activity of the labeled D-fructose was located equally at carbons 1 and 6.

Potassium D-arabonate-5-C^{14} was also prepared from D-mannitol-1-C^{14} in 52-percent yield (26-percent radiochemical yield) without the intermediate separation of crystalline D-fructose-1,6-C^{14}; it was then converted to D-arabinose-5-C^{14} in an over-all radiochemical yield of 18 percent of the original D-mannitol-1-C^{14}.

1. Introduction

Previous reports from this laboratory [1, 2] [3] have described the preparation of 1-C^{14}-labeled mannose, the reduction of this to D-mannitol, and the oxidation of the D-mannitol by *A. suboxidans* to labeled D-fructose. As the two halves of the mannitol molecule are stereomerically alike, oxidation by *A. suboxidans* can take place either at carbon 2 or at carbon 5. If oxidation took place without either an isotope effect or breakdown of the D-mannitol and resynthesis of the fragments, the derived D-fructose would be labeled equally and exclusively at carbons 1 and 6. The present report presents evidence that this fructose is, within experimental error, labeled equally and exclusively at carbons 1 and 6, and describes convenient methods for determining carbon 14 at these positions.

2. Discussion of Experimental Work

Ordinarily, considerable difficulty is experienced in the purification of D-fructose. In the course of the work on the labeled sugar, a convenient procedure was developed for the crystallization of D-fructose from crude sirups. This consists of dehydration of the sugar sirup by azeotropic distillation with absolute ethanol, followed by dissolution in about two parts of methanol, and addition of a higher alcohol such as butanol or isoamyl alcohol to the point of incipient turbidity. After nucleation, the solution slowly deposits large crystals of D-fructose.

For assay of carbon 1 of D-fructose, the method chosen was an alkaline degradation of the sugar in the presence of molecular oxygen [3, 4] adapted to a semimicro scale and so conducted as to avoid contact of the sugar and alkali except under oxygen pressure. The resulting D-arabonic acid was conveniently separated as crystalline potassium D-arabonate, and the assay of carbon 1 of the labeled D-fructose was obtained fron the difference in activity of the sugar and the potassium salt. The method is convenient, and can be used for the assay of carbon 1 of any simple aldose or 2-ketose by choice of a suitable derivative for separation of the lower sugar acid. For the assay of carbon 6 of D-fructose, the potassium D-arabonate described above was oxidized with sodium periodate, and the formaldehyde, which was derived only from the terminal carbinol carbon, was isolated directly from the oxidation mixture by means of the dimedone compound. The procedure is somewhat similar to that used by Reeves [5] for the quantitative determination of the primary carbinol groups of sugars; it does not require distillation of formaldehyde prior to formation of the dimedone compound. The method is suitable for the assay of the terminal carbinol group of any aldonic acid or simple sugar. Although aldoses can be assayed directly by the periodate oxidation method described here, direct assay of ketoses is not practicable because they contain two primary carbinol groups. Thus assay of ketoses by alkaline oxidation to the lower aldonic acid, and periodate oxidation of this, is particularly advantageous.

The C^{14}-labeled D-fructose, assayed as described above, yielded potassium D-arabonate with a molecular loss of 50 percent of the activity. The formaldehyde-dimedone derivative obtained after periodate oxidation accounted for all of the activity of

---

[1] Part of a project on the development of methods for the synthesis of radioactive carbohydrates, sponsored by the Atomic Energy Commission.

[2] The term "D-fructose-1,6-C^{14}" covers all materials labeled in positions 1 and 6, regardless of the proportion of the labels. As the fructose used in this work was prepared from D-mannitol-1-C^{14}, positions 1 and 6 are not labeled in the same molecule.

[3] Figures in brackets indicate the literature references at the end of this paper.

the potassium D-arabonate. Thus the original D-fructose was labeled equally and exclusively in positions 1 and 6.

The methods for the assay of carbon 1 of D-fructose can be used without change for the assay of glucose and mannose. By alkaline degradation in the presence of oxygen, it was shown that all of the activity of a sample of D-glucose-1-C^{14} prepared by the cyanohydrin synthesis from D-arabinose and radioactive cyanide is, unquestionably, located at carbon 1.

The semimicro procedure developed for the preparation of potassium D-arabonate-1-C^{14} is useful, also, for the preparation of D-arabonic-5-C^{14} acid and D-arabinose-5-C^{14}. In the preparation of these substances it is unnecessary to separate crystalline D-fructose after oxidation of D-mannitol by *A. suboxidans*. The fermentation mixture, after deproteinization, deionization, and alkaline oxidation, gave potassium D-arabonate in 52.4-percent yield, based on the D-mannitol fermented. However, because one-half of the activity was lost in removal of carbon 1, the carbon 14 recovered as potassium D-arabonate was 26.2 percent. The potassium D-arabonate-5-C^{14} was converted to D-arabonic-5-C^{14} lactone and this was reduced to D-arabinose-5-C^{14} in 69-percent yield by the procedure developed for the preparation of D-arabinose-1-C^{14} [6]. Obviously, the 5-labeled D-arabinose provides a starting material for the preparation of D-glucose-6-C^{14} and D-mannose-6-C^{14}.

3. Experimental Details

3.1. Purification of D-Fructose

For purification, 180 mg of crude, labeled D-fructose was dissolved in a few drops of water, and the solution was filtered through a microfilter, containing some decolorizing carbon, into a 50-ml round-bottomed flask. The funnel was carefully washed, and the combined solution and washings, after the addition of a drop of acetic acid, were concentrated under reduced pressure to a thick syrup at a temperature less than 35° C. The sirup was dissolved in absolute ethanol, and the solution was transferred to a heavy-walled test tube and reconcentrated under reduced pressure. The residue was dissolved in methanol, the solution was again evaporated under reduced pressure, and the thick sirup was diluted with 5 or 6 drops of methanol. By cautious addition of a methanol-isoamyl alcohol mixture (1:1), and finally of isoamyl alcohol alone, the volume was increased to approximately 1 ml, and the solution was brought to incipient turbidity. It was then lightly seeded and allowed to stand at room temperature. From time to time additional isoamyl alcohol was cautiously added. At the end of a few days the mother liquor was removed, and the crystals were washed in the tube with ethanol and dried. To recrystallize, the D-fructose was dissolved in methanol, the solution was concentrated under reduced pressure, and methanol and isoamyl alcohol were added as before.

3.2. Assay of Carbon 1 of D-Fructose-1,6-C^{14}

A 75-mg sample of labeled D-fructose having an activity of 2.62 μc per millimole was dissolved in 2 ml of water. The solution was transferred and frozen to a portion of the wall of a 200-ml pressure flask, previously cooled in a dry ice-acetone mixture. On a separate portion of the wall, 2 ml of 2 *N* potassium hydroxide was frozen. The flask was immediately placed on a shaking machine,[4] evacuated, and filled with oxygen under 10 lb of pressure; it was then shaken for 24 hr at room temperature. By this procedure, the solutions of alkali and sugar do not come into contact except in the presence of excess oxygen, and the deleterious effect of alkali upon the sugar in the absence of oxygen is avoided. After 24 hr, 50 ml of methanol was added and the solution was lightly seeded with dust of crystalline potassium D-arabonate and allowed to stand for 1 day. The mother liquor was decanted from the crystals, which adhered to the walls of the flask, and the crystals were carefully washed with methanol. The potassium D-arabonate was recrystallized once in the flask by dissolving it in a minimum quantity of water and adding methanol to the point of incipient turbidity. From time to time additional methanol was added to effect more complete crystallization. After 1 day the mother liquor was removed with a capillary pipette. The crystals were washed with methanol and then dissolved in water. The solution was removed from the flask, filtered through a microfilter containing some decolorizing carbon, and concentrated to approximately 1 ml in a small test tube under a stream of dry air; methanol was then added to the point of incipient turbidity. After crystallization had taken place, the mother liquor was removed by means of a capillary pipette, and the product was washed with 50-percent aqueous methanol. The potassium D-arabonate was recrystallized several times from water, by the addition of methanol, to give a product with an activity of 1.32 μc per millimole. This value was unchanged by further recrystallization. Thus the loss in activity accompanying removal of carbon 1 was 49.6 percent.

It was later found that the potassium D-arabonate could be purified to constant activity with 2 or 3 recrystallizations, if the final crystallization was conducted slowly by allowing an aqueous solution in a small test tube to stand undisturbed in a desiccator containing anhydrous calcium sulfate and also a beaker of methanol. In the course of 1 or 2 days large pure crystals formed. The activity of these was unchanged by an additional recrystallization.

3.3. Assay of Carbon 6 of D-Fructose-1,6-C^{14} (Carbon 5 of D-Arabonic Acid)

For the assay of carbon 6 of the labeled D-fructose, potassium D-arabonate was prepared and purified as described above, and then treated in the following manner:

[4] A Parr reduction apparatus (shaking device equipped with a low-pressure gas tank).

A 20-mg quantity of the labeled potassium D-arabonate having an activity of 1.18 μc per millimole was treated with 1.5 ml of 0.3 *N* sodium metaperiodate, and the oxidation mixture, in a glass-stoppered tube, was allowed to stand for 3 hr at room temperature. Aqueous sodium bisulfite was added dropwise in an amount sufficient to cause removal of the iodine that first appeared. The solution was neutralized to the end point of methyl orange by the dropwise addition of aqueous sodium bicarbonate. To the reaction mixture was added 2.5 ml of a freshly prepared solution containing 35 mg of dimedone and 35 mg of sodium bicarbonate. After the solution was carefully neutralized with aqueous hydrochloric acid to the end point of methyl orange, a voluminous crystallization took place. The product was separated and washed with water.

For recrystallization, the material on the filter was dissolved in the minimum quantity of methanol; the solution was passed through the filter and diluted with an equal volume of water. After one recrystallization, the dimedone compound had an activity of 1.20 μc per millimole, which was unchanged by further recrystallization. Thus, within the limits of error, the activity of the dimedone compound accounted for all of the activity of the potassium D-arabonate. Inasmuch as formaldehyde is derived, during the periodate oxidation, only from carbon 5 of the D-arabonic acid (carbon 6 of the parent D-fructose), 50 percent of the activity of the labeled D-fructose was found at carbon 6.

3.4. Assay of Carbon 1 of D-Glucose-1-C^{14}

The alkaline oxidation previously described was also carried out on D-glucose-1-C^{14} having an activity of 3.46 μc per millimole. In this case the potassium D-arabonate obtained was expected to be inactive. The salt was recrystallized once in the pressure flask and once in a small test tube by addition of methanol to an aqueous solution. Finally, the material in aqueous solution was filtered, and allowed to crystallize slowly, as described in section 3.2. The product thus obtained showed negligible activity (0.001 μc per millimole). Hence the parent sugar was labeled exclusively at carbon 1.

3.5. Preparation of Potassium D-Arabonate-5-C^{14} from d-Mannitol-1-C^{14}

A sterile solution consisting of 2 millimoles of D-mannitol-1-C^{14} (having 150 μc of radioactivity), 100 mg of yeast extract, 60 mg of potassium dihydrogen phosphate, and 20 ml of water was incubated at 30° C with a freshly prepared culture of *A. suboxidans*. (The surface to volume ratio was 1.6 cm^2/ml.) After 45 hr, 2 ml of a 20-percent solution of zinc sulfate was added, and then an equivalent quantity of aqueous barium hydroxide. The resulting precipitate was separated by filtration through a funnel heavily coated with diatomaceous earth and decolorizing carbon. The filtrate was concentrated to a volume of about 5 ml, and then frozen on the wall of a 200-ml pressure flask. (The volume with washings was about 8 ml.) Eight milliliters of 2 *N* potassium hydroxide was frozen on another portion of the wall, and the oxidation was conducted as described in section 3.2. The resulting solution was diluted with 5 volumes of ethanol and allowed to stand 24 hr for the crystallization of potassium D-arabonate. After separation and recrystallization, the product weighed 214 mg (52.4-percent yield).

3.6. Preparation of D-Arabinose-5-C^{14}

One millimole (204 mg) of potassium D-arabonate-5-C^{14} was dissolved in 10 ml of water and passed through a column containing 10 ml of cation exchange resin;[5] this was followed by 20 ml of wash water. The effluent was concentrated to a sirup under reduced pressure, and the sirup was transferred to a reduction tube such as that described in [7]. The sugar acid was lactonized by heating it in a current of air at 50° C for several days, with occasional addition of methanol. When the product had become entirely crystalline (about 1 week), the tube was immersed in an ice bath and connected with a stirrer, which reached to the bottom of the tube. After the addition of 3.2 g of crystalline sodium acid oxalate and 10 ml of water, vigorous stirring was begun, and 4.6 g of 5-percent sodium amalgam pellets was added through the sidearm of the reduction tube. Stirring was continued until the amalgam was spent, after which the mercury was separated. Five volumes of methanol was added; the crystalline sodium salts were separated by filtration, washed with methanol, and discarded. The alcoholic solution was concentrated under reduced pressure to about 5 ml, 25 ml of methanol was added, and the solution was filtered to remove a second crop of nonradioactive sodium salts. The solution was concentrated to remove the methanol, and was neutralized at ice temperature with sodium hydroxide to the end point of phenolphthalein. A small crop of nonradioactive salts was removed, and the solution was then passed through an ion-exchange column containing equal parts of cation and anion exchange resins.[6] The salt-free and neutral effluent was concentrated to 100 ml under reduced pressure, and finally was freeze-dried. The residue was dissolved in 0.5 ml of methanol, and isopropanol was added to the point of incipient turbidity. Crystallization of D-arabinose-5-C^{14} progressed readily, and ultimately 103 mg of crystalline D-arabinose was separated without the addition of carrier (yield=68.6 percent).[7] As potassium D-arabonate was obtained in 52.4-percent yield from D-mannitol, with the elimination of one-half of the carbon 14, the over-all radiochemical yield of D-arabinose-5-C^{14} was 18 percent.

[5] Amberlite IR 120, Rohm & Haas Co., Philadelphia, Pa.
[6] Amberlite IR 100, analytical grade, Rohm & Haas Co., Philadelphia, Pa., and Duolite A-4, Chemical Process Co., Redwood City, Calif.
[7] There has been considerable variation in yield in this preparation; a radiochemical yield of 60 to 70 percent may be expected.

4. References

[1] H. S. Isbell, J. V. Karabinos, H. L. Frush, N. B. Holt, A. Schwebel, and T. T. Galkowski, J. Research NBS **48,** 163 (1952) RP2301.

[2] H. S. Isbell and J. V. Karabinos, J. Research NBS **48,** 438 (1952) RP2334.

[3] O. Spengler and A. Pfannenstiel, Z. Ver. deut. Zucker-Ind. **85,** 546 (1933).

[4] H. S. Isbell, J. Research NBS **29,** 227 (1942) RP1497.

[5] R. E. Reeves, J. Am. Chem. Soc. **63,** 1476 (1941).

[6] H. L. Frush and H. S. Isbell, U. S. Atomic Energy Commission Report No. NBS–2309 (1953); J. Research NBS **51** (December 1953) (in press).

[7] H. L. Frush and H. S. Isbell, U. S. Atomic Energy Commission Report No. NBS–1752 (1952); J. Research NBS **50,** 133 (1953) RP2400.

WASHINGTON, July 22, 1953.

Journal of Research of the National Bureau of Standards Vol. 51, No. 4, October 1953 Research Paper 2447

Measurement of Variations in Atmospheric Refractive Index With an Airborne Microwave Refractometer[1]

Howard E. Bussey and George Birnbaum

A microwave refractometer for aircraft use is described, and some of the sources of error in the measurement of variations of atmospheric refractive index with this instrument are discussed. Observations were made up to 10,000 feet on 2 days near Washington, D. C. Two refractive-index soundings taken 1½ hours apart showed changes that, in the coarser aspects, resembled changes shown by radiosonde data. The fluctuation intensity changed erratically with time and place, but was usually greatest where the vertical gradient was changing. A rough analysis of the data showed that the larger fluctuations occurred over distances of several hundred meters, whereas over distances less than 5 meters the fluctuations were negligible (the response of the instrument would have allowed the detection of fluctuations occurring within 0.5 meter). Large increases in index were observed on entering cumulus clouds and intense fluctuations were noted within the clouds.

1. Introduction

Experience shows that meter- and centimeter-length electromagnetic waves are propagated far beyond the horizon [1, 1a] [2] with a field strength much greater than what can be accounted for on the basis of standard diffraction theory [2]. To explain this discrepancy it has been proposed that the waves are scattered by inhomogeneities in the refractive index of the atmosphere.[3] Consequently, there is need for a detailed knowledge of the refractive-index structure of the atmosphere, especially with regard to sharp changes in the vertical gradient and irregular local variations from the mean value. Apart from these considerations, observations of refractive-index variations in the upper atmosphere are of interest in their own right in meteorological science, especially because of their close relation to the water-vapor structure there.

Many observations of atmospheric refractive index have been made recently with an airborne microwave refractometer by Crain and coworkers [4]. A few observations with an airborne microwave refractometer of somewhat different design are reported here. Except for modifications necessitated by aircraft installation, this instrument was essentially that developed by Birnbaum [5] and used for observations near the ground [6, 7]. Special attention was given to the problem of measuring rapid fluctuations as there is virtually no information available on refractive-index inhomogeneities of small extent.

This paper describes the essential features of the airborne instrument and its performance, exhibits selected portions of the data obtained on a flight up to 10,000 ft and through clouds, presents the results of a crude statistical treatment of the data, and discusses the experiment in relation to previous meteorological measurements.

[1] Parts of this paper were presented at the Third Radar-Weather Conference, McGill University, Montreal, Canada, Sept. 1952, and at the Joint Meeting of URSI and IRE, Washington, D. C., April 1953.

[2] Figures in brackets refer to literature references at the end of this paper.

[3] A review of radio-wave scattering by the atmosphere has been published by Megaw [3].

2. Description of Equipment

The frequency change, Δf, of a cavity resonator due to a refractive-index change, Δn, of the air contained therein is expressed to a very good approximation by

$$-\Delta f/f=\Delta n.$$

As in this work Δn is of the order of 10^{-6}, it is convenient to introduce a quantity ΔN defined by

$$\Delta N=\Delta n\times 10^{6},$$

where N is called an N-unit. Δf is measured by electronically comparing the frequencies of a ventilated (test) cavity and a sealed (reference) cavity. These are excited by a frequency-modulated klystron, and their outputs after detection yield resonance curves that are used to control the width of a rectangular voltage waveform. This voltage is averaged, amplified, and recorded.

The design of the instrument constructed for aircraft operation differed somewhat from that described [5, 6] in previous reports. The klystron (type 2K25) was isolated from the large pressure changes encountered in ascents and descents by sealing its mount. An available power supply originally designed for 60-c/s input voltage operated satisfactorily with the 800-c/s voltage supplied by the aircraft. The klystron sweep voltage was synchronized to the aircraft mains, and consequently, the time constants of the electronic circuits were adjusted for a pulse repetition rate of 800 c/s.

The sampling cavity [4] was installed at a location believed to be in free air, undisturbed by turbulence along the fuselage. It was attached on the end of a streamlined boom (fig. 1) 3.7 ft long located 6.7 ft from the nose of the aircraft (a Navy type P4Y2). The waveguide lead to the cavity was inside the boom. The electronic circuits, reference cavity, and klystron located nearby were shock-mounted. As further protection from aircraft vibration, low micro-

[4] This and the reference cavity operated in the TE_{011} mode at 9,000 Mc.

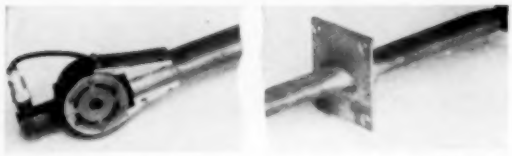

FIGURE 1. *Sampling cavity attached to the end of the strut.*

phonic tubes (12AY7) were employed in the input stages of the resonance pulse amplifiers. Connection between the shock-mounted waveguide and the rigidly mounted waveguide in the boom was effected by a short length of flexible coaxial cable.

The reference cavity was provided with a small diameter plunger driven by a micrometer whose scale was calibrated in terms of cavity frequency change. By means of this plunger the refractometer was calibrated, also the recording pen was reset whenever it approached the off-scale position. The latter adjustment permitted the use of a sensitive scale to determine fine detail, yet preserved the much larger changes in refractive index that occurred in a sounding.

Invar of high purity that had been subjected to a special heat treatment [8] was used in the construction of the test cavity in order to minimize thermal expansion. The treated metal had a measured coefficient of linear expansion of 0.3×10^{-6}/° C., and the finished cavity had the same coefficient because the change in the refractometer reading due to heating of the cavity was $0.3N$/° C.[5] However, after installing the cavity in the aircraft the coefficient increased to 0.5×10^{-6}/° C. It is felt that this was due to stressing by the aluminum supports. The reference cavity available from previous work was temperature compensated to within 0.5×10^{-6}/° C by using brass end plates suitably recessed into an untreated invar ($\alpha=3\times10^{-6}$/° C) barrel.

Possible changes in air density arising from the rapid passage of air through the cavity were investigated at speeds up to 170 mph. The test cavity was mounted in the NBS wind tunnel and changes of air density in the cavity were deduced from measurements with the refractometer. Within the experimental error of 0.5 to $1N$ caused by constant addition of fresh air to the tunnel, the densities of air within tunnel and cavity were alike.

The smoothing of air-temperature fluctuations due to contact of air with the cavity walls was determined in previous laboratory tests for air speeds up to 25 mph. At this speed the amplitude of air-temperature fluctuations was reduced by 20 percent; but at aircraft speeds the reduction should be negligible.

The ability of the refractometer to record rapid changes in index clearly depends on the repetition rate of the klystron sweep voltage. Thus for a sweep rate of f (equal to 800 c/s in the present case), oscillations at a frequency of $f/2$ should be detected and the shape of those at $f/6$ or less should be well

[5] $\Delta f/f=-\alpha$, where α is the linear-expansion coefficient.

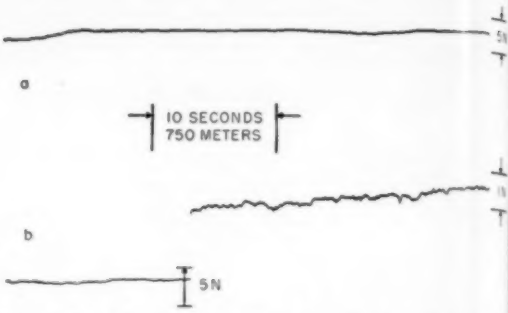

FIGURE 2. *Two segments of the refractive-index record obtained while in level flight in very homogeneous air at about 10,000 foot altitude.*

reproduced. The response time of the present equipment, however, was found to be limited by that of the recording milliammeter.[6] The response of the recorder was essentially flat out to 20 c/s, and decreased by a factor of one-half at 45 c/s.

While making atmospheric observations a constant chart speed of 2.5 mm/sec was used. Consequently oscillations more rapid than 10 c/s would not be individually resolved. They would, however, broaden the trace if they were continuously present as the recorder could respond to higher frequencies. The trace width was normally ⅓ mm, which was equivalent to $0.05N$ on the most sensitive range used, $7N$ full scale. On the basis that an 80-percent broadening of the trace was easily visible and taking account of the decrease in recorder response at higher frequencies, it was estimated that the minimum amplitude of index oscillation necessary for detection at various frequencies was as indicated in table 1.

TABLE 1.

Frequency	Minimum detectible amplitude	Length
c/s	*N*	*m*
10	0.02	4
75	.04	0.5
375	.5	.1

The length there is the distance traversed by the aircraft (whose speed was 75 m/sec) during a half cycle of the oscillation. It indicates the approximate "size" of the index inhomogeneity that would give rise to the frequency in question.

The smallest refractive-index fluctuation that can be reliably observed is limited by noise originating within the equipment. In the laboratory a maximum noise amplitude of $0.05N$ was observed, and this occurred in intervals of the order of 1 to 2 sec. There were virtually no current variations visible in

[6] By strongly modulating the screen voltage of one of the amplifiers, the width of the refractometer rectangular pulse, and hence output current, was made to vary sinusoidally.

½-sec intervals or shorter. In flight it was not convenient to seal the ventilated cavity in order to obtain a record of equipment noise. Instead, an upper limit of this noise was estimated by assuming that it alone was responsible for the variations in the smoothest section of the data. Figure 2 shows two such records obtained in very homogeneous air at 10,000 ft. The deviation from the mean in ¼-sec intervals was about $0.02N$ and in 1-sec intervals about $0.07N$.

No effort was made to determine the longtime stability of the equipment. This depends in large measure, however, on the thermal expansion of the cavities as the temperature environment changes. The observed temperature change in the ascent to 10,000 ft was large enough to give an indicated change of several N-units. Some variation might occur also from drift in klystron center frequency with temperature, as the klystron was not thermostatically controlled. In addition, pressure changes during ascent might shift the frequency of the sealed cavity slightly. Although these effects could cause errors of perhaps 5 percent in the sounding, they do not influence the reliability of the observations of fluctuations.

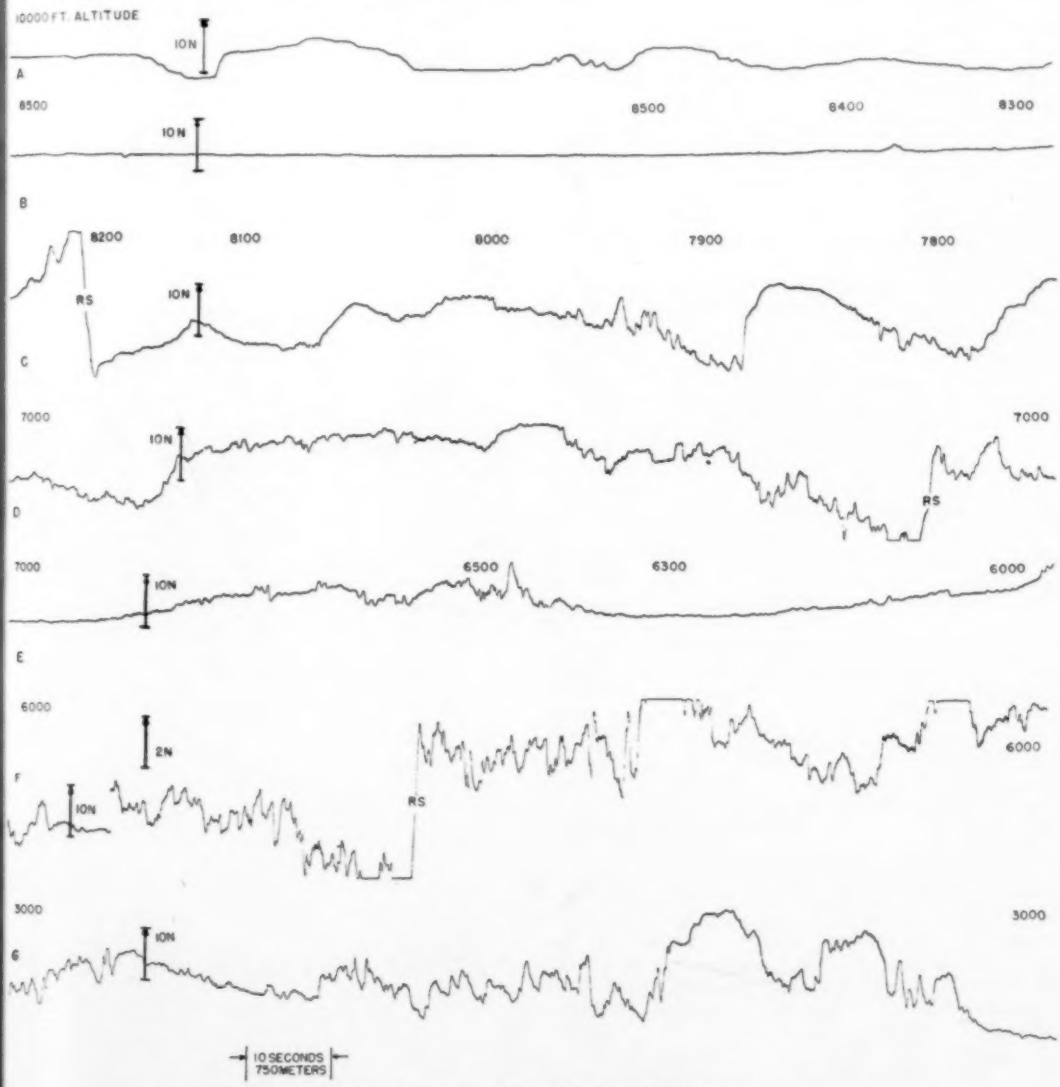

FIGURE 3. *Examples of refractive-index data.*

The length of each strip represents the passage of 126 seconds in time or about 10 kilometers in distance.

3. Results

The observations described in this section were obtained over the Chesapeake Bay within 12 miles of North Beach, Md., on August 19, 1952, from 1300 to 1600 EST. The weather was warm and humid. There was a 15-mph north wind up to about 8,000 ft, and above this level there was a 25-mph west wind. The radiosonde temperature profile indicated a dry adiabatic lapse rate (neutral equilibrium) up to 4,000 ft and a moist adiabatic lapse rate above 4,000 ft. The presence of scattered cumulus clouds with bases at 4,000 ft and tops at 12,000 to 14,000 ft was evidence of large-scale vertical convection processes.

3.1. Description of Data

The horizontal speed of the aircraft was kept to about 75 m/sec (170 mph) and during a sounding the ascent or descent rate was held to about 2.5 m/sec. Thus the slope of the inclined path was about one-thirtieth. In figure 3 are shown sections of strip charts, each of which is 126 sec in duration. During this time the aircraft traveled 10 km horizontally, and, if making a sounding, changed altitude by 300 m.

Although the atmosphere at 10,000 ft was for the most part smooth and homogeneous, as shown in figure 2, there was a short time when it was not, as is illustrated in figure 3, a. This figure shows the occurrence of slow variations of appreciable amplitude, but with virtually none of the rapid fluctuations that were usually observed at lower levels.

Figure 3, b, illustrates the pronounced and widespread uniformity of refractive index that was encountered from 8,500 to 8,300 ft (during the descent), and which persisted for the most part up to 10,000 ft the highest altitude explored.

Figure 3, c, shows a very large increase in index, namely, $25N$, between 8,300 and 8,100 ft. (The pen went off scale during this increase and was reset at the place marked RS.) This region of fast transition was caused by a widespread and persistent stratification of the atmosphere. It was observed during four ascents or descents within a half-hour period and was always encountered at the same height to within ± 100 ft. This apparent boundary between two air masses was visible as a sharply defined haze line, with comparatively clear air above. This would indicate, in agreement with the large variation of index, that the air was moist below the transition and dry above it.

Another striking feature of this record is the smooth and very rapid increase of $10N$ at 7,900 ft. This increase, which represents one of the sharpest boundaries encountered, occurred within 0.7 sec, during which time the aircraft traveled 50 m horizontally and descended 2 m. The index then slowly returned to about its former value in a horizontal distance of 2,500 m.

At 7,000 ft the plane was leveled for horizontal flight. Fluctuations of various durations and amplitudes occurred (fig. 3, d), but most interesting of all was a well-defined refractive-index variation that extended about 5 miles and had a mean amplitude of about $12N$.

Figure 3, e, was obtained in descending from 7,000 to 6,000 ft.

An example of a record in which the full-scale sensitivity was changed from 33 to $7N$ is shown in figure 3, f, although in general the index variations were too great to permit the use of the more sensitive scale. No perceptible broadening of the stylus trace occurred on changing sensitivity, indicating that continuous fluctuations with durations of 0.1 to 0.0 sec (7.5 to 1.5 m) were of amplitude less than 0.03 The smallest fluctuations that are plainly visible have amplitudes of 0.1 to $0.2N$ and durations of 0. sec. There are many fluctuations of 1 to $2N$ with durations of a few seconds.

At 3,000 ft the fluctuations (fig. 3, g) were definitely of greater amplitude than at the higher elevations. The strikingly large-amplitude and long-duration fluctuations near the end of the record are indicative of large and rather homogeneous eddies of air whose refractive index differs markedly from the mean. As will be indicated later, these variations as well as those of smaller amplitude arise chiefly from variations in vapor density.

3.2. Refractive Index of Clouds

Refractive-index observations were made at 7,0 ft while flying through some fair-weather cumulus clouds. These had bases at roughly 4,000 ft and tops in the neighborhood of 12,000 to 14,000 ft. The air temperature inside and outside the clouds was approximately the same, 13.5° C. On entering a rather well-developed cloud the refractive index increased by about $40N$ and then fluctuated violently (fig. 4, a). The increase that can be seen in the figure amounts to $16N$, but while the trace was off scale (marked A) the frequency of the reference cavity was changed by an amount equivalent to 30 in an attempt to set the pen on scale. Then the

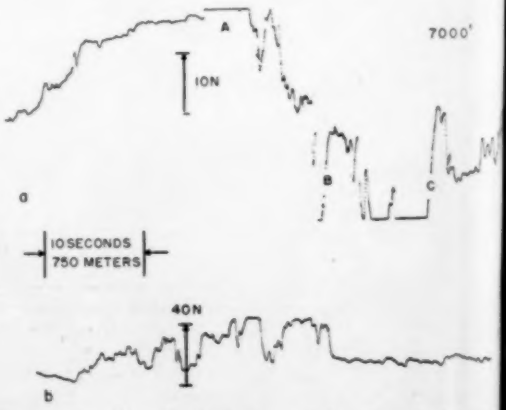

FIGURE 4. *Records obtained on flying through fair-weather cumulus clouds.*

index suddenly decreased and went off scale as the most dense part of the cloud was passed. The trace was reset at points B and C. By taking into account the displacements of the tuning plunger, it was seen that after leaving the cloud the refractive index returned to its original value. Changes of 6 to 10N within a distance of about 25 m were observed in the cloud. Further evidence of the great turbulence that existed there were the bumps experienced by the aircraft. By way of contrast, it may be mentioned that a moderate bump was encountered in clear air with no noticeable change in index.

On entering another cloud not as well developed as the first, the index increased by 35N; and on leaving, decreased by this amount (fig. 4, b). In this case the full-scale sensitivity was 135N. Inside the cloud several changes as large as 20N were noticed.

Remarkably sharp refractive-index gradients were observed in both clouds; changes of 12 to 15N within a distance of 12 m occurred in three or four instances and of 6N within 2 m in one instance.

While circling at 10,000 ft, where the refractive index was quite uniform, it was noticed that a definite increase occurred as a nearby cloud was passed. The distance of closest approach to the cloud was 1 or 2 miles.

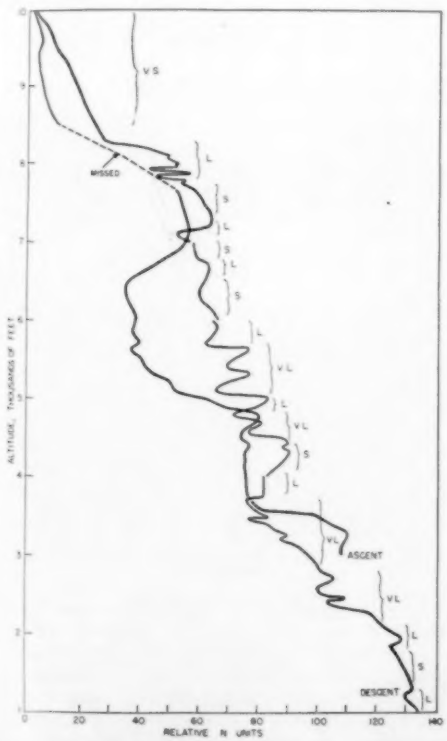

FIGURE 5. *A smoothed ascent sounding, and a descent sounding taken about 1½ hours later.*

Breaks in the descent curve occur due to interruption of the descent for horizontal explorations. The adjectives describing the rapid fluctuations (applicable to the descent curve only) represent amplitudes approximately as follows: VS, very small, 0.25N or less; S, small, 0.5N; L, large, 1.0N; VL, very large, 2.0N or more.

3.3. Refractive-Index Profiles

To obtain the variation of refractive index with height, the original data were smoothed by obtaining visually sucessive 10-sec averages. Curves plotted from such values are shown in figure 5. Included there are rough estimates of the mean amplitude of those fluctuations less than 5 sec in duration. On comparing these estimated amplitudes with the gradient, one notices the not surprising result that regions of change of gradient are associated with large fluctuation amplitudes.

One of the curves in figure 5 is based on data taken in ascent and the other on data taken in descent about 1½ hr later. During this interval the refractive index clearly increased at all levels above 5,000 ft. For comparison, refractive-index profiles computed from radiosonde data are shown in figure 6. These data [7] were obtained in the vicinity of Silver Hill, Md., in the morning and evening of the day of the flight. The increase in index during this longer interval is somewhat greater than that noted above. This increase as shown by the radiosonde data must have been due almost entirely to changes in water-vapor density, as the temperature and pressure profiles scarcely changed.

[7] Supplied by the U. S. Weather Bureau.

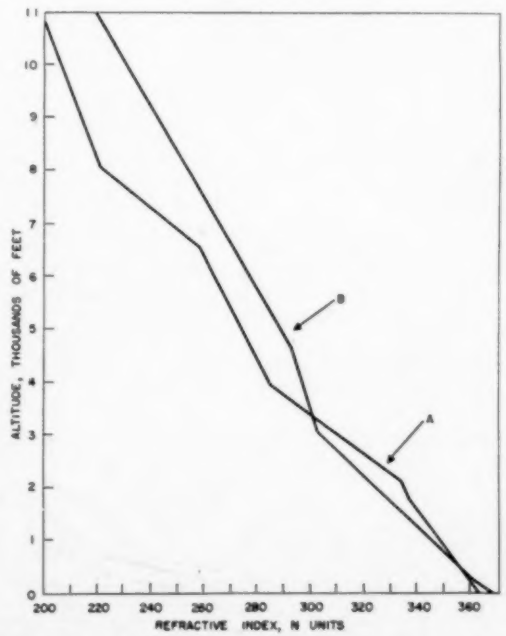

FIGURE 6. *Refractive-index profiles for Washington, D. C., August 19, 1952, calculated from radiosonde ascents.*
a, 1000 EST; b, 2200 ETS.

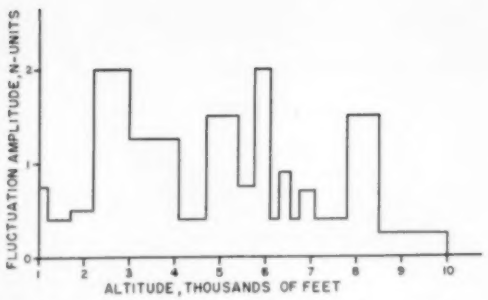

FIGURE 7. *Amplitude of fluctuations of medium-sized parcels as a function of altitude*

4. Data Analysis

This section presents the results of a rough statistical treatment of the data based upon the following considerations. The atmosphere may be regarded as an assembly of air parcels whose refractive-index values differ from one another and in general from the mean value. Within any large parcel there may be smaller parcels of smaller index variations and so on. The refractive-index amplitude of a parcel was taken as the peak positive or negative deviation from the local mean and the extent or size, in the direction of flight, as the interval between consecutive intersections of the record with the local mean. A rough estimate was made of the percentage of time that parcels of various sizes appeared to be present. The duration of the local running mean was adjusted in proportion to the size of the parcels to be analyzed. The results are expected to be roughly related to Fourier amplitudes and periods as might be obtained by usual statistical methods.

The results of the data analysis are summarized in table 2, which shows that both the amplitude and percentage of time present increase with the size of the parcel. In a few cases, where level flights in a given direction were made, sizes greater than the 6,000 m indicated in table 2 were observed. Indeed, the presence of air parcels some 10 to 30 miles in extent has been detected by aircraft measurements of temperature and vapor pressure [9, 10].

TABLE 2. *Estimates of extents and amplitudes of the refractive-index inhomogeneities (parcels)*

Altitude	Extent	Average amplitude	Time present
ft	*m*	*N*	%
1,000 to 8,000	10 to 20	0.2	40
	40 to 80	1.0	60
	100 to 200	1.5	80
	2,000 to 6,000	4.5	100
8,500 to 10,000	10 to 15	0.04	50
	20 to 30	.1	80
	200 to 300	.25	80

The 1,000-m range of sizes at altitudes above 8,500 ft were not included in table 2. Variations in the altitude of the aircraft over such distances could have caused the small refractive-index variations observed.

For parcel sizes of the order of several hundred meters, the variation of amplitude with height is shown in figure 7. In this particular case there is certainly no clear systematic variation. It should be noted that the amplitudes for the region 1,000 to 8,000 ft in table 2 are averaged over the wide variations indicated by figure 7.

An important finding of this analysis was the fact that the amplitude of the refractive-index inhomogeneities of small extent was extremely small. From the absence of broadening of the trace while the sensitivity was $7N$ full scale, it was concluded that sizes in the range of 0.5 to 5 m, if present, had amplitudes no greater than $0.04N$. There were some 10 instances in the flight where this more sensitive scale was used. In addition there was an initial test flight (made on August 15), with most of the data recorded at 10,000 ft, which also showed the absence of trace broadening within the limits specified above. As for the remainder of the present flight, taken with a full-scale sensitivity of $33N$, from the absence of trace broadening it can only be stated that 5-m sizes, if present, had amplitudes less than $0.1N$ at all times.

5. Discussion

5.1. Causes of Refractive-Index Fluctuations

For the mean conditions of temperature, vapor pressure, and total pressure encountered in the flight, the change in refractive index, Δn, is approximately related to the change in temperature, ΔT(° C), and to the change in vapor pressure, Δe(mm Hg) by [8]

$$\Delta n \times 10^6 = \Delta N = 6\Delta e - \Delta T.$$

Rapid pressure fluctuations are too small to influence ΔN. Radiosonde records [9] taken at Silver Hill, Md., on the day of the flight were examined, and it was found that ΔT fluctuations for sizes that the radiosonde can best detect—50 to 100 m—were usually less than 0.2 deg C, thus accounting for only a fraction of ΔN for these sizes (see table 2). It is probable that for other sizes also the changes of index were mainly due to changes of vapor pressure. This view is supported by the measurements of reference [4].

5.2. Clouds

The large increases in N observed in the clouds are reasonably accounted for on the basis of changes in water-vapor content. The uprising saturated air in the clouds at a temperature of 13.5 ° C should have a refractive-index value about $70N$ greater than if it were dry. As shown by radiosonde data, the relative humidity outside the cloud at 7,000 ft was about 40 percent. The observed increases of 35 to $40N$ in

[8] This result was obtained from the expression $(n-1)10^6=103.5\ P/T+4.97\times10^5\ e/T^2$, using representative values of the variables. (P is the total pressure in mm Hg.)

[9] Provided by the U. S. Weather Bureau. The time constant (4 sec) should allow parcels of dimensions (in the vertical direction) of 50 to 100 m to be detected.

the clouds are therefore reasonable. The liquid droplets in these clouds would contribute a small amount to the index—less than $1N$. An artificial effect due to deposition of liquid drops on the cavity walls does not appear likely because of the rapidity of the observed variations. The existence of large amplitude fluctuations within the cumulus cloud may be evidence of the process called entrainment [11], in which surrounding drier air mixes with the uprising saturated air of the cloud.

The index inhomogeneity in the clouds was so great that it was wondered whether appreciable radar return could result. The back-scattering cross section per unit volume is given by $\overline{\Delta n^2}/8\pi l$ [15] where l, the scale of turbulence, is large compared to the radar wavelength. From the data it was estimated that l was of the order 100 m, and $\overline{\Delta n^2}$ was 10^{-10}. These values yield a cross section of 4×10^{-16} cm^2/cm^3. For 10-cm-wavelength radiation, this result is about 100 times larger than that expected due to Rayleigh scattering from rainless clouds [10] in which the mean drop diameter is 0.001 cm, but even so, it amounts to only a very small scattering cross section capable of detection only at a short range—of the order of 1 mile.

5.3. Soundings

The ascent and descent soundings (fig. 5) differ not only as to the aspect of the coarse gradient but also as to the amount of fine structure. The ascent was made immediately after low-lying stratus clouds were dissipated by the sun's heating and may have taken place before the onset of strong vertical mixing. The subsequent descent shows greater inhomogeneity, such as might have been caused by widespread vertical mixing.

It should be realized that the various changes of gradient in a sounding may be due to three causes: (1) a rather permanent stratification,[11] (2) a temporary or fluctuating gradient, and (3) an artificial effect that occurs because the angle of ascent is small, thus allowing horizontal gradients to give rise to apparent vertical gradients. The existence of permanent layers can, of course, be confirmed by repeated soundings as was done in connection with the layer boundary at 8,300 ft. The large gradient observed in ascent at 3,500 ft may also have represented a layer boundary, but this was not checked.

5.4. Index Parcels of Small Size

In the present work it was found that the fluctuation amplitude associated with an index parcel decreased with the size of the parcel. In fact, the amplitudes of 5-m parcels (and smaller) were found to be negligible. A similar finding was reported by Crain et al. [4], although their observations did not extend to as small a parcel size as observed here. These results, although of limited scope, lend some support to Megaw's [14] assumption, made in connection with his theory of atmospheric scattering of radio waves, of a (Kolmogoroff) spectrum of parcel sizes terminated at 10 cm by viscosity on the small-size end. Booker and Gordon [15], in dealing with radio-wave scattering, used a scale or mean parcel size of 10 cm with an amplitude of $1N$, but no such parcels were observed in the present experiments.

[10] It appears that Friend [12] may have detected rainless clouds with 10-cm radar.

[11] Stable stratifications of water vapor in the atmosphere have been observed by Dobson, Brewer, and Cwilong [13], using an airborne dew-point hygrometer.

6. Conclusions

Although a limited amount of data was taken, the results served to demonstrate the operation of the instrument and to give some notions about the refractive-index structure of the atmosphere. It was found that the character of the fluctuations changed erratically with position and time. A persistent feature of the two flights was the absence of very rapid fluctuations. Quantitatively expressed, it was found that fluctuations that occurred in distances of from 0.5 to 5 m had an amplitude less than 0.04×10^{-6} in n (or $0.04N$). The larger amplitude fluctuations occurred over distances of the order of 1,000 m, which interestingly enough is in general agreement with the mean scale of turbulence of 300 m for the atmosphere obtained by Megaw [14] from stellar scintillation data, and with horizontal dimensions of 2,000 to 3,000 m of some of the parcels observed by Bunker [16].

The measurements described here were made in cooperation with the Naval Research Laboratory and the aircraft was furnished by that laboratory. We express our gratitude for the cooperation extended to us by the members of the Wave Propagation Research Branch, and especially to R. E. Katz, who aided in several phases of the experiment and to H. D. Metke, who piloted the aircraft. A. Hanyok constructed the electronic equipment. We also thank H. Lyons, K. A. Norton, and J. W. Herbstreit for their interest.

7. References

[1] M. Katzin, R. W. Bauchman, and W. Binnion, 3- and 9-cm propagation in low ocean ducts, Proc. IRE **35,** 891 (1949).

[1a] J. W. Herbstreit, K. A. Norton, P. L. Rice, and G. E. Schafer, Radio wave scattering in tropospheric propagation, IRE Convention Record, part 2, (New York, N. Y., 1953).

[2] W. Miller, Effective earth's radius for radiowave propagation beyond the horizon, J. Appl. Phys. **22,** 55 (1951).

[3] E. C. S. Megaw, Waves and fluctuations, J. Inst. Elec. Engrs. (London) **100,** 1 (1953).

[4] C. M. Crain, A. P. Deam, and J. R. Gerhardt, Measurement of tropospheric index-of-refraction fluctuations and profiles, Proc. IRE **41,** 284 (1953). See also Refractometer measured tropospheric index-of-refraction profiles, **I,** Univ. of Texas, Elec. Engr. Res. Lab. (Feb. 1953).

[5] G. Birnbaum, A recording microwave refractometer, Rev. Sci. Instr. **21,** 169 (1950).

[6] G. Birnbaum, Fluctuations in the refractive index of the atmosphere at microwave frequencies, Phys. Rev. **82,** 110 (1951).

[7] G. Birnbaum, H. E. Bussey, and R. R. Larson, The microwave measurement of variations in atmospheric refractive index, Trans. IRE, Prof. Group on antennas and propagation, No. 3, p. 74 (Aug. 1952).
[8] B. S. Lement, B. L. Averbach, and M. Cohen, The dimensional behavior of invar, Trans. Am. Soc. Metals **43,** 1072 (1951). See also, Rev. Sci. Instr. **22,** 196 (1951).
[9] R. Frith, Meteorological research flight, Meteorol. Mag. **77,** 3 (1951).
[10] P. A. Langwell, Inhomogeneities of turbulence, temperature, and moisture in the West Indies trade wind region, J. Meteorol. **5,** 243 (1948).
[11] E. W. Barrell and H. Riehl, Experimental verification of entrainment of air into cumulus clouds, J. Meteorol. **5,** 304 (1948).
[12] A. W. Friend, Theory and practice of tropospheric sounding by radar, Proc. IRE **37,** 116 (1949).
[13] G. M. B. Dobson, A. W. Brewer, and B. M. Cwilong, Meteorology of the lower atmosphere, Proc. Royal Soc. (London) [A], **185,** 144 (1946).
[14] E. C. S. Megaw, Scattering of electromagnetic waves by atmospheric turbulence, Nature **166,** 1100 (1950).
[15] H. G. Booker and W. Gordon, A theory of radio scattering in the troposphere, Proc. IRE **38,** 401 (1950).
[16] A. F. Bunker, Diffusion, entrainment, and frictional drag associated with non-saturated buoyant air parcels rising through a turbulent air mass, J. Meteorol. **10,** 212 (1953).

WASHINGTON, July 1, 1953.

Journal of Research of the National Bureau of Standards Vol. 51, No. 4, October 1953 Research Paper 2448

Studies in the System Magnesia-Silica-Water at Elevated Temperatures and Pressures

Elmer T. Carlson, Richard B. Peppler, and Lansing S. Wells

The reactions between magnesia and silica under hydrothermal and pneumatolytic conditions were investigated. Chrysotile and talc were produced, depending on the ratio of the reacting oxides. The chrysotile was submicroscopic but was shown by the electron microscope to have a fibrous structure. Chrysotile and talc were likewise prepared from mixtures of magnesium carbonate and silica. The same products were obtained by the action of silica in the vapor phase on solid magnesia. A detailed study of this method was made, and the effects of temperature, pressure, time, pH, and oxide ratio on the amount of silica transported were determined. The overall rate of transport was found to increase with temperature, pressure, and pH.

1. Introduction

The system MgO-SiO_2-H_2O has been the subject of extensive study by a considerable number of investigators over a period of many years. This widespread interest is in part due to a desire to explain the mechanism of the formation in nature of the various hydrated magnesium silicate minerals, particularly serpentine. Probably a stronger motive for much of the research has been the hope of developing a method for the practical synthesis of serpentine in its fibrous form, chrysotile, which is the most important of the asbestos minerals.

The various terms applied to the serpentine minerals are not used in the same way by all investigators. In this report no attempt will be made to justify the terminology employed, but the mineral names will be used in accordance with what appears to be most common usage. The word *serpentine* will be applied in general to the mineral or to synthetic preparations having the approximate composition $3MgO{\cdot}2SiO_2{\cdot}2H_2O$. The terms *chrysotile* and *antigorite* will be applied respectively to the fibrous and the platy crystalline forms of serpentine. These two forms presumably differ in their internal structure, but the X-ray patterns that have been published have many features in common, and often are not free from ambiguity.

Magnesia and silica have been found to combine readily in the presence of water vapor, especially at elevated temperatures and pressures. Among the products obtained is a compound having the chemical composition of chrysotile, but never its fibrous habit, so far as can be seen with the light microscope. Bowen and Tuttle [1],[1] in their study of the system MgO-SiO_2-H_2O, showed by differential thermal analysis, and other means, that this actually is chrysotile. Electron photomicrographs showed that the crystals were definitely rod shaped. These authors also showed that chrysotile may be formed at temperatures below 500° C, but not above, and at pressures from 2,000 to 40,000 lb/in^2.

One of the ultimate objects of the present work was the preparation of chrysotile fibers of larger size. This attempt proved unsuccessful, but some of the information obtained appears of sufficient value to be recorded.

As a preliminary step in this investigation, an exhaustive search was made of the literature pertaining to asbestos, as well as to the system MgO-SiO_2-H_2O and related subjects. A bibliography of selected references has been compiled.[2]

2. Experimental Studies

2.1. Solubility of Magnesia

As a starting point it was considered desirable to know the solubility of the reactants at elevated temperatures. The solubility of silica in water has already been investigated thoroughly over the range from 0° to 425° C, and at pressures up to 1,250 atm. The available data being adequate, no further work was done in this field.

The situation with respect to magnesia is quite different. A considerable number of investigations of the solubility of magnesia at and near room temperature have been made, but the data vary over a wide range. It has been shown that the solubility of magnesia varies with the temperature at which it was prepared, and varies also if it was prepared at a given temperature from different materials. Gjaldbaek [2], in 1925, concluded that there is an unstable, soluble form of $Mg(OH)_2$ which first forms and is quickly converted to a stable, less soluble form.

There appears to have been only one investigation of the solubility of $Mg(OH)_2$ in the absence of CO_2 and at temperatures above the melting point of water. This is the work of Travers and Nouvel [3] in 1929, wherein the solubility of $Mg(OH)_2$ was investigated in the range from 0° to 200° C. The description of their method is very brief, and nothing is said about filtration of high-temperature solutions. It therefore seemed advisable to investigate the

[1] Figures in brackets indicate the literature references at the end of this paper.

[2] A limited number of single copies are available from the authors.

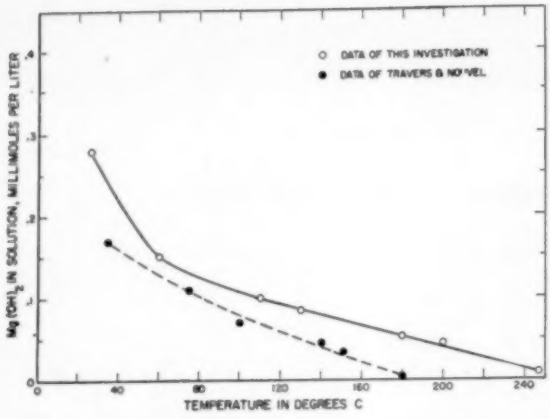

FIGURE 1. *Solubility of magnesia in water at various temperatures.*

solubility of magnesia over as wide a temperature range as possible.

The solubility determinations were made on the same MgO that was used in subsequent synthesis experiments. It was of laboratory quality and had been previously ignited for 1 hr at 1,000° C. It was found to contain 0.2 percent of extraneous soluble salts. A series of solubility determinations were also made on another portion of this same MgO that had been extracted with water and that had not been previously ignited. The values obtained with this MgO were slightly but consistently lower than those obtained with the ignited and unwashed MgO.

The water used in each case was ordinary distilled water, the CO_2 content of which had been decreased by boiling and bubbling CO_2-free air through it. A few determinations were made, using water that had not been treated in this fashion, and the solubilities thus obtained were consistently slightly higher.

Solubility determinations were made at seven different temperatures in the range 30° to 250° C. The determinations at temperatures under 100° C were made in rubber-stoppered polyethylene bottles, that were stored, with occasional shaking, in electrically heated ovens maintained at the desired temperature. Portions of these solutions were taken from time to time and analyzed until a value was obtained that did not change for several days. The MgO was determined by titration against standard HCl, using methyl red as an indicator.

For the determinations at temperatures above 100°, use was made of an autoclave of special design described in an earlier paper [4]. This autoclave was of stainless steel, with a capacity of 2 liters, and was fitted with a Munroe filter, which permitted filtration of the solution before the autoclave was opened. Aliquots were analyzed as described above.

The data are presented in table 1 and plotted in figure 1. The solubility was found to decrease steadily from 2.1×10^{-4} mole per liter at 30° to 1×10^{-5} mole per liter at 250°.

TABLE 1. *Solubility of $Mg(OH)_2$ in water at various temperatures*

Experiment	Type of MgO	Temperature	Time	Solubility as $Mg(OH)_2$
		° C	*Days*	*Millimole/Liter*
1	Washed	30	10	0.21
2	Ignited	30	4	.28
3	Washed	60	9	.14
4	Ignited	60	7	.16
5	do	110	10	.10
6	do	130	12	.08
7	do	180	10	.05
8	do	200	10	.04
9	do	245	10	.01

In the determinations at 30° and at 60° C there was an initial supersaturation lasting about a day. When a series of samples at 30° C were tumbled continuously on a suitable mechanical tumbler, the duration of the period of supersaturation was greatly reduced but the magnitude remained about the same. Because the actual shape of the solubility-versus-time graphs is a function of technique used, they are not reproduced in this paper.

At the lowest temperatures there was an appreciable difference between the data obtained for the washed and for the unwashed ignited magnesia. As the temperature increased, the difference decreased; accordingly, at temperatures above 100° C, only one kind, the ignited MgO, was used.

In the temperature range 100° to 250° C the solubility of magnesia steadily decreases (fig. 1). The smallest value, 1×10^{-5} mole/liter, is the limit of usefulness of this method of analysis, for thereafter the area of confusion in the end point is of the same order of magnitude as the titration.

The data of Travers and Nouvel [3] are also plotted in figure 1. It may be observed that their data are of the same order of magnitude as those obtained in this investigation, but consistently lower. Because these investigators do not describe the magnesia they used nor what precautions, if any, were taken to remove CO_2 from the solutions, one cannot comment on this difference.

For the purpose of this investigation it was not considered desirable to extend these solubility determinations to higher temperatures. It is apparent that the solubility of $Mg(OH)_2$ will become immeasurably small before even the minimum temperature of the subsequent synthesis experiments is reached.

2.2. Synthesis Experiments

a. Materials and Methods

For most of the experimental work the magnesia used was reagent quality magnesium oxide. This was found to be hydrated to a considerable, and variable, extent. Calcium in soluble form was found to be present to the extent of 0.17 percent, expressed as CaO. No attempt was made to determine the actual calcium compounds present. It was not considered necessary to purify the magnesia further by extraction with water. Failure to do so, however, gave rise to some confusing results, to be

described later. The magnesia was used either in the partially hydrated state or after ignition at selected temperatures.

For a few experiments, reagent quality magnesium carbonate was used. Analysis indicated that it was actually the basic carbonate, hydromagnesite ($3MgCO_3 \cdot Mg(OH)_2 \cdot 3H_2O$).

Several forms of silica, including silica gel, powdered flint, and quartz, were used. For the majority of the experiments the silica was present as reagent grade silicic acid. Ordinary distilled water was used.

Pressure bombs of the Morey type served as reaction vessels. These were made of stainless steel, and had an average capacity of about 18 ml. They were heated in vertical-tube resistance furnaces with pyrometric control, using iron-constantan couples. In most cases the fluctuation in temperature over a period of a week was within a 4-deg range. Pressure was neither independently controlled nor directly measured. The values given for pressure in tables 2, 3, and 4 were calculated from the temperature and the ratio of the quantity of water to the volume of the vessel. The charge was placed in a small platinum crucible supported above the bottom of the bomb. For the vapor-transport experiments, only the magnesia was placed in the crucible, the silica being put in the bomb cavity beneath. In these cases the crucible was left uncovered, and as a rule no water was added directly to the magnesia. Except where otherwise stated, the quantity of water in the bomb was approximately the amount that would be completely converted to steam just below the critical temperature.

After removal from the furnace, the bomb was cooled in air, in front of a fan, and opened. The charge was then dried at about 110° C, and examined under the polarizing microscope. X-ray diffraction analysis and other tests were then made, if desired. X-ray patterns were made on an X-ray Geiger-counter diffractometer, using copper K_α radiation.

b. Experiments with Mixtures of Magnesia and Silica

Several series of experiments were conducted on intimate mixtures of magnesia and silica, both in the 3:2 molar ratio required for serpentine and in the 3:4 ratio of talc. Data for a few of these experiments are presented in table 2, the rest having been omitted because they contributed no additional information of significance.

The reaction products always appeared amorphous when viewed under the microscope, except that there was often some birefringence, especially in products formed at the higher temperatures and in the more siliceous mixtures. The index of refraction was close to 1.56 in all cases. By means of X-ray diffraction patterns it was shown that crystalline material was produced. After 1 day at 200° C, a mixture of magnesia and silicic acid in 3:2 molar ratio gave a very weak diffraction pattern with diffuse bands. Higher temperatures and longer heating periods resulted in stronger patterns. After 7 days at 250°, a strong pattern was obtained, and similar results were found at higher temperatures.

TABLE 2. *Data of hydrothermal experiments on mixtures of magnesia and silica*

Experiment	Molar ratio $MgO:SiO_2$	Initial state of MgO	Temperature	Pressure	Time	Product
			°C	*atm*	*Days*	
1	3:2	MgO	200	15	1	Chrysotile (diffuse X-ray pattern).
2	3:2	do	250	39	7	Chrysotile.
3	3:2	do	300	85	7	Do.
4	3:2	do	380	235	7	Do.
5	3:2	do	412	315	4	Do.
6	3:2	do	470	365	3	Do.
7	3:2	$MgCO_3$[a]	348	159	7	Chrysotile; a little $MgCO_3$.
8	3:2	do	373	215	5	Chrysotile.
9	3:2	$MgCO_3 \cdot 3H_2O$[b]	404	300	13	Do.
10	3:4	MgO	301	86	7	Talc.
11	3:4	do	368	293	7	Do.
12	3:4	do	422	315	7	Do.
13	3:4	$MgCO_3$[a]	299	84	7	Do.
14	3:4	do	419	310	7	Do.

[a] Reagent quality magnesium carbonate, found by analysis to be basic magnesium carbonate (hydromagnesite, $3MgCO_3 \cdot Mg(OH)_2 \cdot 3H_2O$).
[b] Synthetic.

In these cases the pattern was essentially identical with one given by a specimen of natural chrysotile asbestos.

Similar results were obtained when magnesium carbonate was substituted for magnesium oxide in the mixtures. The silica displaced the CO_2 from the carbonate.

Mixtures of magnesia and silica in 3:4 ratio produced talc at all temperatures tried.

In a series of experiments with the 3:2 mixture, very small amounts of various other substances were added. These included compounds of various metals that are known to occur in natural serpentine, also ammonia, ammonium salts, volatile acids, and NaOH. In no case was there any evidence of fibrous structure in the product.

c. Vapor Transport Experiments

It has been shown that silica is appreciably soluble in water-vapor, both above and below the critical temperature. Synthesis of serpentine through the action of vapor-borne silica on $Mg(OH)_2$ has been reported by Syromyatnikov [5] and van Nieuwenburg [6]. It appeared desirable to make a study of this method of synthesis, with special attention to the effect of temperature and various other conditions on the rate of transport of silica.

For these experiments a weighed quantity of MgO was placed in a small open crucible supported near the top of the bomb chamber, and the silica and water were placed in the bottom of the chamber. After the desired period of heating, the crucible and contents were removed, dried, ignited at 1,100° C, and weighed. The increase in weight was ascribed to SiO_2. In one case the silica was determined by actual analysis, with good agreement as to results.

An attempt was made to evaluate separately the effects of relative proportion of the oxides, temperature, pressure, and pH on the rate of transport of silica to the magnesia. In order to accomplish this, it was first necessary to determine whether the

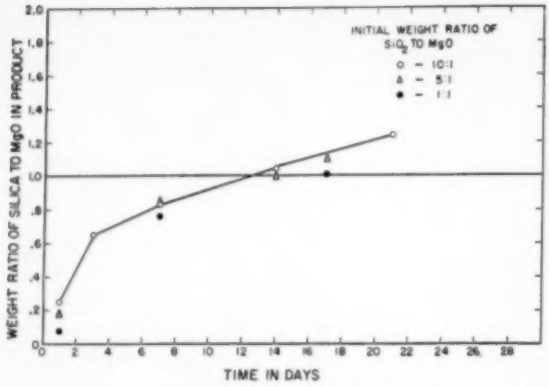

FIGURE 2. *Effect on silica transport of varying the initial ratio of silica to magnesia.*

results were reproducible. This was found to be the case, within reasonable limits, provided all experimental conditions were fixed. Results obtained in one furnace did not always agree with those obtained in a different furnace. Specifically, two of the furnaces were found to give results differing widely from all the others. This is believed to be due to a difference in temperature gradient. In the majority of the furnaces the temperature at the base of the bomb was found to be about 2 deg higher than that at the top. The two exceptions mentioned above appeared to have a slight gradient in the opposite direction. In these, the transport of silica was negligible. The data recorded below represent experiments in five furnaces giving reasonably concordant results.

d. Effect of proportion of oxides.

A temperature of 380° C was arbitrarily chosen and a series of determinations made, using the apparatus and techniques described earlier. Using three initial proportions of silica to magnesia, namely, 10 to 1, 5 to 1, and 1 to 1, and in all cases, 4 g of water in the bombs, the amount of silica transported to the magnesia was determined at various times. The results obtained are shown in table 3 and figure 2.

The spread of the values shown in figure 2 is within the limits of experimental error, and it is therefore concluded that, providing a certain minimum amount of silica is present, the transport of silica to magnesia is independent of the relative amounts of silica and magnesia. The amount of silica used in all cases was sufficient to cover the bottom of the bomb. It may be that the available surface area of the silica is a significant factor, but this was not investigated. It was observed that the smaller the absolute amount of silica initially present, the greater was the weight percent of it that was transported under the same conditions of temperature and time. This is to be expected.

TABLE 3. *Silica-transport isotherms*

Experiment	Time	Weight of SiO_2	Weight of MgO	Initial SiO_2/MgO, by weight	Weight of SiO_2 transported	SiO_2/MgO in product by weight
(1) 360° C isotherm. Pressure 189 atm.						
	Days	*g*	*g*		*g*	
1	2	0.9845	0.0981	10.04	0.0183	0.19
2	7	.9874	.1112	8.88	.0400	.36
3	14	.9830	.0789	12.46	.0421	.53
4	21	.9838	.0864	11.38	.0946	1.09
(2) 380° C isotherm. Pressure 235 atm.						
5	1	1.0036	0.1046	9.59	0.0267	0.25
6	1	.9994	.100	9.99	.0265	.26
7	1	.100	.1150	.87	.0080	.08
8	1	.500	.0965	5.18	.0170	.18
9	3	1.0000	.100	10.00	.0650	.65
10	7	1.0038	.1027	9.77	.0848	.83
11	7	.5036	.100	5.04	.0851	.85
12	7	.1022	.100	1.02	.0760	.76
13	7	.4834	.100	4.83	.0945	.94
14	14	1.000	.1077	9.29	.1078	1.00
15	14	.5052	.100	5.05	.100	1.00
16	14	1.000	.0960	10.42	.1085	1.13
17	14	1.000	.0965	10.39	.1006	1.04
18	21	1.0007	.1060	9.44	.1311	1.24
19	21	.100	.0994	1.01	.0971	.98
20	21	.500	.0990	5.05	.1130	1.10
21	28	.9961	.0933	10.67	.1597	1.71
(3) 400° C isotherm. Pressure 274 atm.						
22	1	0.9910	0.0892	11.14	0.0107	0.12
23	3	.9965	.0909	11.00	.0304	.33
24	8	1.000	.0988	10.12	.0837	.85
25	8	1.000	.1067	9.37	.0864	.81
26	8	.9757	.0960	10.16	.0564	.59
27	12	1.000	.1052	9.51	.1092	1.04
28	14	1.000	.0957	10.45	.1118	1.17
29	14	.9953	.0934	10.66	.1183	1.26
30	21	1.000	.0957	10.45	.1434	1.50
(4) 420° C isotherm. Pressure 312 atm.						
31	3	0.9928	0.0987	9.75	0.0328	0.33
32	9	.9833	.0930	10.57	.1091	1.17
33	14	.9849	.0998	10.17	.1385	1.43
34	21	1.000	.1037	9.64	.1553	1.50
35	21	1.000	.0970	10.31	.1583	1.63

It was further observed that, within the limits of these experiments, the identities of the reaction products of the magnesia and the transported silica were not a function of the initial proportions of silica and magnesia. These reaction products are discussed later.

Effects of time and temperature. Four temperatures were arbitrarily chosen, namely, 360°, 380°, 400°, and 420° C, and determinations were made of the silica transported to magnesia after 3, 7, 14, and 21 days at each of these temperatures.

The initial proportion of silica to magnesia was 10 to 1 in each case, and the bomb contained 4 g of water. Because the amount of water used was constant, the pressures that obtained in the bombs varied with the temperature and also in the case of the postcritical temperatures with the ratio of the volume of water to that of the bomb cavity. The bombs used were fairly uniform in capacity, and for this work were considered identical. Each isotherm then had its own characteristic pressure. These pressures were, for the four temperatures of 360°, 380°, 400°, and 420°, respectively, 189, 235, 274, and 312 atm.

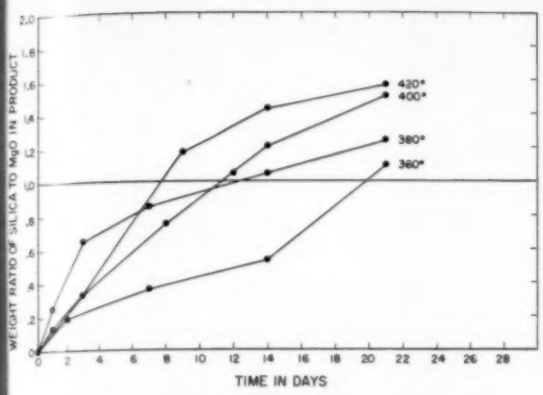

FIGURE 3. *Silica transport at various temperatures.*

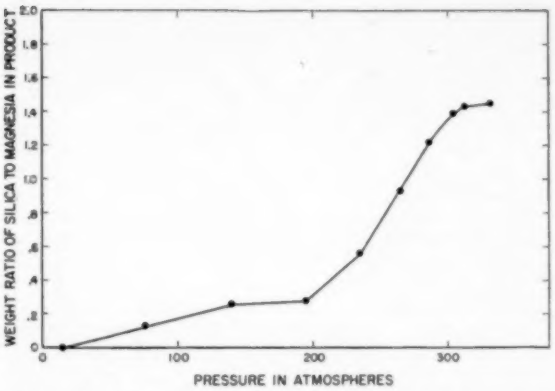

FIGURE 4. *Effect of pressure on silica transport at a constant temperature of 420° C and a contsant time of 14 days.*

The data obtained from these experiments are presented in table 3 and figure 3. In figure 3 it may be observed that the amount of silica transported increases with increasing time at each temperature and that it increases with increasing temperature. It may further be observed that the three postcritical isotherms are of the same type, showing rapid early transport of silica relative to the transport at the one precritical temperature. The identity of the reaction products between the magnesia and the transported silica is not a function of temperature in this range. These will be discussed later.

Effect of pressure. A temperature of 420° C and a time of 14 days were arbitrarily chosen to study the effect of pressure on silica transport. The same apparatus and techniques previously described were used. The pressure was varied from 15 to 600 atm by varying the degree of filling of the bomb with water. The actual values of the pressure under these varying circumstances were obtained by interpolation in the tables given by Van Nieuwenburg and Blumendal [7]. It was found that at pressures above 330 atm, in the particular equipment that was used, the transport of extraneous material from the bombs and metal gaskets made it impossible to obtain quantitative data. For this reason, data obtained at pressures above 330 atm are not included in this report.

The results of these determinations are presented in table 4 and figure 4. Referring to figure 4, it may be observed that the amount of silica transported at 420° C increases with increasing pressure, gradually at first, then very rapidly in the pressure range of 200 to 300 atm, after which it begins to level off.

The distribution and proportions of the reaction products depend on the amount of silica transported and consequently on pressure, temperature, and time, but the identity of these products is not a function of these variables in the ranges investigated.

These reaction products were examined with the petrographic microscope, and X-ray powder patterns were made of samples taken from different depths in

TABLE 4. *Effect on silica transport of varying the pressure at constant temperature of 420° C and constant time of 14 days*

Experiment	Weight of silica	Weight of MgO	Initial SiO_2/MgO, by weight	Weight of H_2O	Pressure	Weight of silica transported	SiO_2/MgO in product, by weight
	g	*g*		*g*	*atm*	*g*	
1	1.1195	0.1072	12.19	0.10	15	0.0002	0.00
2	1.1100	.1142	12.61	.50	76	.0145	.13
3	1.1218	.0899	12.58	1.00	140	.0216	.24
4	1.0006	.0910	10.99	1.00	140	.0253	.28
5	1.1108	.0903	12.64	1.50	195	.0246	.27
6	1.1360	.0976	12.25	2.00	234	.0552	.56
7	0.9694	.1040	10.05	2.50	266	.0864	.93
8	.9735	.0990	8.03	3.00	286	.1212	1.22
9	.9993	.0960	10.41	3.50	303	.1335	1.39
10	.9849	.0968	10.17	4.00	312	.1385	1.43
11	.9985	.1053	9.48	5.00	332	.1555	1.48
12	1.1300	.1056	12.35	5.00	332	.1493	1.41

the platinum thimble containing the charge. Only three compounds were formed, namely, chrysotile, talc, and brucite.

In general, talc predominated in the silica-rich surface of the reaction product, and its proportion increased with increasing amount of silica transported. The chrysotile occurred as microcrystals visible under the electron microscope only, but giving a sharp X-ray diffraction pattern. Brucite always predominated in the bottom half of the reaction product and sometimes also in the upper half, depending on the amount of silica that had been transported. In the investigation of effect of pressure at 420° C, it was found that the proportion of talc and chrysotile in the bottom half of the reaction product was greater at lower pressures.

Effect of pH. The effect of increasing the pH on the transport of silica to magnesia was investigated at 420° C and a constant period of 14 days. In each case the proportion of silica to magnesia initially present was 10 to 1, the absolute amounts being 1 and 0.1 g, respectively, and the amount of water present was 4 g.

The pH was not measured as such but was varied by adding increasing proportions of NaOH to the silica initially present. The experiments were otherwise identical with those previously described. It was found that the transport of silica was not affected until the molar ratio of NaOH to silica initially present was about 0.15 and that the amount of silica transported thereafter increased with increasing NaOH. When the initial NaOH to silica molar ratio was 0.32, the amount of silica transported had increased about 64 percent over what was transported under the same conditions without any NaOH being present.

The NaOH appeared to have no effect on the reaction product other than what could be expected by increasing the amount of silica transported, that is, increasing the proportion of talc.

Because of experimental difficulties involved in accurately weighing NaOH and because pH cannot be directly measured under these conditions, only a few determinations were made.

Effect of calcium present as an impurity. During some preliminary experiments on this method of synthesis, a new crystalline product was observed, and the same material was found in minute quantities in a considerable number of later preparations. It consisted of slender, flexible fibers, occasionally 2 mm or more in length. The refractive indices, 1.584 to 1.594, were somewhat higher than those usually given for chrysotile, although the values found in the literature vary over a wide range. Because of the possibility that these crystals might be chrysotile, a great deal of work was done in an attempt to increase the yield. At the same time, it was suspected that the fibers might prove to be the hydrated calcium silicate, xonotlite, because the refractive indices were about right for this compound. Addition of small quantities of lime to the magnesia appeared to have no effect. However, an increased yield of the fibrous crystals was obtained by substituting dolomitic lime for the magnesia, but the amount was still too small for identification. After much futile experimentation, a product was obtained containing a few tenths of a milligram of the fibrous crystals, which could be separated mechanically from the rest of the material. X-ray analysis proved them to be xonotlite. Although it was known that the magnesia contained some calcium (equivalent to 0.17 percent of CaO), the amount of the latter was so slight that the formation of calcium silicate crystals of conspicuous size was somewhat surprising. It was estimated that the calcium must have been quantitatively converted in order to account for the amount of xonotlite produced.

Miscellaneous experiments. The experiments discussed above were designed to bring out in a systematic manner the effects of varying certain experimental conditions. A variety of other experiments were performed, in a qualitative way, in an attempt to promote the growth of crystals of chrysotile of larger size. For example, the magnesia was made into a paste and coated on the crucible or on other supports of various shapes. Again, the period of hydrothermal treatment was increased to 45 days. Traces of various acids and of compounds of various metals were added, both to the silica and to the magnesia. In no case were any microscopically visible crystals of chrysotile produced.

Silica in the vapor phase was found to react with magnesium carbonate at 380° C, with formation of chrysotile and talc. Natural serpentine was partially altered to talc by exposure to siliceous vapor for 7 days at 380°, but not at 350°. Under similar conditions, at 380°, olivine showed evidence of surface attack.

In another series of four experiments, an attempt was made to increase the size of fragments of natural chrysotile asbestos fibers. Bundles of fibers were cut to a length of about 0.03 inch and treated hydrothermally under four conditions: (a) on the surface of a bed of MgO; (b) imbedded in MgO; (c) imbedded in a mixture of MgO and SiO_2 in 3:2 ratio; (d) packed into cavities in magnesite. Treatment was for 14 days at 420° C, with 3 g of water in the bomb; other conditions were as described previously for the vapor-transport experiments. No change in the size or appearance of the chrysotile fibers was observed.

3. Summary

Magnesia and silica in 3:2 ratio were found to combine under hydrothermal conditions at temperatures as low as 200° C. X-ray and electron microscope studies showed that the product was chrysotile, but the fibrous crystals were too small to be distinguished as such by light microscopy.

Chrysotile, together with talc, was also formed by the action of siliceous vapor on magnesia. Conditions governing the rate of transport of the silica were worked out in considerable detail. The rate was found to increase with temperature and pressure and also with the initial pH. No improvement in crystal size resulted from this method of synthesis.

Silica was found to displace CO_2 from $MgCO_3$ under hydrothermal conditions at 380°.

The X-ray diffraction patterns were prepared by B. M. Sullivan and G. M. Ugrinic, of the Constitution and Microstructure Section. Their valuable assistance is acknowledged with thanks.

4. References

[1] N. L. Bowen and O. F. Tuttle, Bul. Geol. Soc. Am. **60,** 439 (1949).
[2] J. K. Gjaldbaek, Z. anorg. Chem. **144,** 145 (1925).
[3] A. Travers and Nouvel, Compt. rend. **188,** 499 (1929).
[4] E. P. Flint, H. F. McMurdie, and L. S. Wells, J. Research NBS **21,** 617 (1938) RP1147.
[5] F. V. Syromyatnikov, Econ. Geol. **30,** 89 (1935).
[6] C. J. van Nieuwenburg, Rev. gen. sci. appl. (Brussels) **1,** 61 (1952).
[7] C. J. van Nieuwenburg and H. B. Blumendal, Rec. trav. chim. **51,** 707 (1932).

Washington, July 16, 1953.

Journal of Research of the National Bureau of Standards Vol. 51, No. 4, October 1953 Research Paper 2449

Dielectric Properties of Teflon from Room Temperature to 314° C and from Frequencies of 10^2 to 10^5 c/s[1]

Paul Ehrlich[2]

The dielectric constant and dissipation factor of Teflon were measured at frequencies from 10^2 to 10^5 c/s and from room temperature to temperatures just below the first-order transition point occurring at 327° C. Measurements of the d-c conductivity were made over the same temperature interval. Results show that the dielectric constant decreases somewhat with increasing temperature. The relation between thermal-expansion coefficient and temperature coefficient of the dielectric constant is roughly as predicted by the Clausius-Mossotti equation. Values of dissipation factor and d-c conductivity at all temperatures are very low (less than 2×10^{-4} and 2×10^{-15} mho/cm, respectively), and the dielectric constant is independent of frequency at all temperatures.

1. Introduction

The dielectric behavior of Teflon, an organic high polymer with outstanding temperature stability, is investigated over a wide temperature range with equipment especially designed to permit measurements at elevated temperatures. Previous qualitative investigations [1][3] have indicated the absence of significant dielectric losses in Teflon up to its first-order transition point at 327° C. No quantitative investigation has been made of the variations of dielectric constant and dielectric loss with temperature This requires the use of a loss-free micrometer sample holder having the characteristics discussed elsewhere [2].

The following symbols are used in this paper. The subscript 0 refers to room-temperature values.

2. Symbols

ϵ' = the dielectric constant.
$\tan\delta$ = the dissipation factor.
$\epsilon''=\epsilon'\times\tan\delta$ = the loss factor.
f = frequency in cycles per second.
$\omega=2\pi f$.
τ = relaxation time.
C_a = the capacitance of a sample of air of the same dimensions as the dielectric measured.
D = the electrode diameter (2 inches).
d = the sample diameter
s = the sample thickness.
C = the capacitance reading on the internal bridge capacitor with the sample holder connected.
C_B = the capacitance reading on the internal bridge capacitor with the sample holder disconnected.
$C_D=C_B-C$ computed at any constant temperature.
ΔC_D = the difference between the room temperature value of C_D and that obtained at another temperature.
C_m = the computed value of the capacitance of the ring of air located between sample and electrode edges, neglecting edge effects.
ΔC_m = the difference between the value of C_m at any temperature and the room temperature value.

[1] Supported by Office of the Chief of Ordnance, Department of the Army.
[2] Present address, Department of Chemistry, Harvard University, Cambridge, Mass.
[3] Figures in brackets indicate the literature references at the end of this paper.

3. Methods

3.1. Electrical Measurements

The measurements of dielectric constant and dissipation factor were carried out by means of a substitution method, changes in sample capacitance with temperature being followed by balancing with the internal bridge capacitor connected in parallel with the sample holder.

In the experiments to be described, the sample capacitance at room temperature was found by making measurements with the sample between the electrodes and with the sample removed from the electrodes. After the temperature was raised, the sample was kept between the electrodes at all times, and drifts in the bridge were compensated for by disconnecting the sample holder after each reading and by reestablishing the balance with the internal bridge capacitor. The disconnecting was accomplished by means of the special switch built into the sample holder. Details of the measuring equipment are described elsewhere [2].

If it is assumed (1) that the sample expands uniformly in all directions, and (2) that the edge effect at all temperatures is effectively eliminated, we obtain

$$\Delta C_M=\frac{0.08854\pi}{4s_0}\left[D^2(1-s_0/s)-d_0^2(1-s/s_0\right], \quad (1)$$

and the dielectric constant at any temperature is found to be

$$\epsilon'=s_0/s\left[\epsilon_0'+(\Delta C_D+\Delta C_m)/C_{a_0}\right]. \quad (2)$$

3.2. Sensitivity and Accuracy of Measurements

The sensitivity of the dielectric constant and dissipation-factor measurements was determined by the sensitivity and stability of the bridge elements, as well as by the ratio of sample capacitance to that of the entire arm, consisting of leads, sample holder, sample, and substitution capacitor. It is estimated

that, for the experiments cited, the overall accuracy of the dielectric-constant computations is probably not determined by the accuracy and sensitivity of the dimensional measurements made at room temperature or by the bridge balance, which could be read to $\pm 0.002 \mu\mu f$. The overall accuracy is determined by deviations from the basic assumptions made, namely, that warping does not take place, that the sample expands uniformly, and that the edge corrections at all temperatures are effectively eliminated. Small deviations from the first two of these assumptions, which are not readily recognizable, are expected to exceed the sensitivity of a room-temperature measurement. It is therefore difficult to make a reliable estimate of the accuracy of the dielectric-constant measurements carried out at higher temperatures. As shown later, the agreement between the several runs was very satisfactory, but an answer to the question of accuracy has to wait for further experiments on samples of widely varying dimensions. The best indication that the dielectric-constant values computed cannot be far from correct is the agreement between the observed and predicted relationship between thermal-expansion coefficient and the temperature coefficient of the dielectric constant. The estimated accuracy of the dissipation-factor measurements is $\pm 1 \times 10^{-4}$. The d-c conductivity never exceeded the smallest observable value of 2×10^{-15} mho/cm.

3.3. Preparation of Specimens

Molded Teflon undergoes drastic dimensional changes when reheated. It was expected that dimensional stability could be attained by conditioning the samples at a temperature above its 327° C first-order transition point. Complete stress relaxation and disappearance of all crystallinity at this temperature has been reported [1], and it was therefore expected that the conditioning process would relieve internal strains introduced during molding. This was borne out by the fact that samples that underwent very drastic changes during conditioning for several hours at 350° C exhibited no further obvious changes when the process was repeated and did not appear to warp during the electrical measurements. Prior to machining, the samples were therefore kept at 350° C for several hours. They were then machined in a vacuum chuck to give disks approximately 1½ in. in diameter and approximately ⅛ in. thick. As measured by calipers, the faces were flat and parallel to ± 0.0003 cm and the diameters constant to ± 0.005 cm, the latter value being determined by the sensitivity of the caliper.

Previous experiments had shown that for accurate measurements over a temperature range it was essential to apply secondary electrodes to the samples. Of the materials tested, evaporated gold was found to be the most satisfactory electrode material, and this was used in all the experiments to be cited.

4. Results and Discussion

Measurements were made on samples A and B cut from different sections of a molded rod. Sample B was reannealed as previously described to give sample C. Sample D had been machined from a disk molded separately and came from a different lot than the rod from which the other samples were cut. The values of the dielectric constant at any temperature were not frequency dependent, as will be demonstrated presently, and the values measured at room temperature for samples A, B, C, and D were 2.002, 1.994, 2.016, and 2.022, respectively. The density of the samples was 2.13.

Table 1 gives results for a typical run (sample A) carried out over the entire temperature and frequency ranges. Values of the dielectric constant have been calculated with the aid of eq (1) and (2). It is seen that the values of the dissipation factor, which are of the order of the sensitivity of the bridge, do not show a trend, either with frequency or with temperature. The dissipation factor can, therefore, be represented as having the value of $(1 \pm 1) \times 10^{-4}$ over the temperature and frequency ranges investigated. Inspection of table 1 also indicates that there is no significant variation of the dielectric constant with frequency at any one temperature. Such a variation would not be expected in view of the very low values of the dissipation factor. The frequency dependence of the dielectric constant can be predicted from the observed values of the loss factor by extending [3] a procedure already described [4] to materials with frequency-independent losses, giving

$$\frac{d\epsilon'}{d \log f} = 2.303 A \epsilon'',$$

where

$$A = \frac{\int_0^{1/\omega} \omega d\tau}{2 \int_0^{1/\omega} \frac{\omega d\tau}{1+\omega^2\tau^2}} = 2/\pi,$$

whence

$$\frac{d\epsilon'}{d \log f} = 1.47 \epsilon''.$$

Thus, for Teflon ($\epsilon' = 2$, $\tan \delta = 1 \times 10^{-4}$), a change in dielectric constant of 0.001 over the frequency interval from 10^2 to 10^5 c/s is computed. This confirms the conclusion, already surmised from table 1, that there is no significant variation of dielectric constant with frequency at any one temperature.

One would expect, therefore, that the variation of dielectric constant with temperature would be caused essentially by the variation in the bulk density of the material. It becomes clear that the accuracy of the dielectric-constant computations depends critically on the validity of the assumptions underlying eq (1)

TABLE 1. *Dielectric constant, dissipation factor, and d-c conductivity of Teflon (sample A)*

Direct-current conductivity (mho/cm) $<2\times10^{-18}$ at all temperatures

Temperature	Frequency	Dielectric constant, ϵ'	Dissipation factor, tan $\delta\times10^4$
°C	c/s		
23	10^2	2.001	1
	10^3	2.002	−2
	10^4	2.003	2
	10^5	2.002	0
86	10^2	1.979	1
	10^3	1.978	1
	10^4	1.980	1
	10^5	1.979	2
113	10^2	1.968	1
	10^3	1.969	2
	10^4	1.969	1
	10^5	1.970	0
136	10^2	1.958	−1
	10^3	1.958	1
	10^4	1.957	1
	10^5	1.959	1
176	10^2	1.942	2
	10^3	1.944	3
	10^4	1.943	1
	10^5	1.942	2
219	10^2	1.902	1
	10^3	1.902	−1
	10^4	1.903	2
	10^5	1.904	1
276	10^2	1.876	−1
	10^3	1.875	1
	10^4	1.875	2
	10^5	1.874	2
314	10^2	1.813	0
	10^3	1.812	1
	10^4	1.810	2
	10^5	1.807	4

and on an accurate determination of the sample thickness at all temperatures. Figure 1 shows a plot of relative sample thickness versus temperature. It is seen that the reproducibility is satisfactory and that the experimental values agree with those reported by one of the manufacturers of Teflon. This may be taken as evidence that warping of the sample did not take place to an extent that would seriously influence the results.

Figure 2 is a plot of dielectric constant versus temperature. An average value of the dielectric constant is used, valid over the entire frequency range and room temperature values of 2.000 have been assumed for each sample in order to obtain a more accurate idea of the reproducibility of the temperature runs. The values used in the plot have therefore been obtained by merely adding or subtracting a small constant correction from the experimental points at all temperatures. As in figure 1, the reproducibility is satisfactory.

The Clausius-Mossotti equation predicts a relation between the temperature coefficient of the static dielectric constant and the linear thermal-expansion coefficient, α_l, which, in the case of a nonpolar material like Teflon, one might expect to be applicable to the dielectric constant at audio and radio frequencies. Similar relations can be derived for other theories, but we shall assume the validity of the Lorentz field and therefore of the Clausius-Mossotti equation, obtaining [5]

$$\frac{d\epsilon'}{dT}=-\alpha_l(\epsilon'-1)(\epsilon'+2)\cdot$$

In the case of Teflon, the value of $-(d\epsilon'/dT)/\alpha_l$ predicted on the basis of the above equation would therefore range from roughly 3.85 at 100° C. to roughly 3.5 at 250° C. The experimental values range from 3.6 at 100° C to 3.0 at 250° C.

In view of the assumptions underlying the evaluation of the experimental dielectric constants, this comparison would seem at least not to be in disagreement with the Clausius-Mossotti theory, although a truly quantitative test on this basis would seem to be impossible.

The sensitivity of the bridge is much too low to obtain even a qualitative idea of the behavior of the dielectric losses as a function of temperature and frequency. Table 1 indicates that the values of the

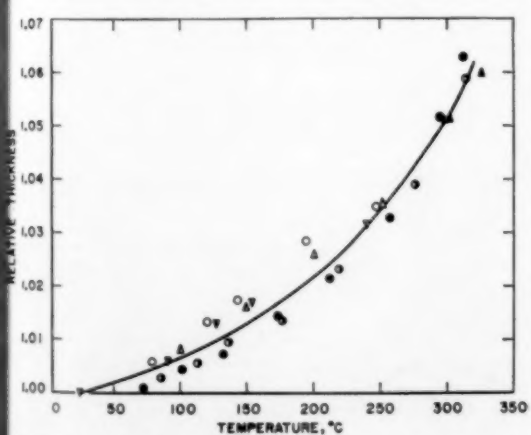

FIGURE 1. *Relative thickness of Teflon as a function of temperatures.*

◑, sample A; ○, sample B; ▽, sample C; ●, sample D; △, expansion measurements made by manufacturer.

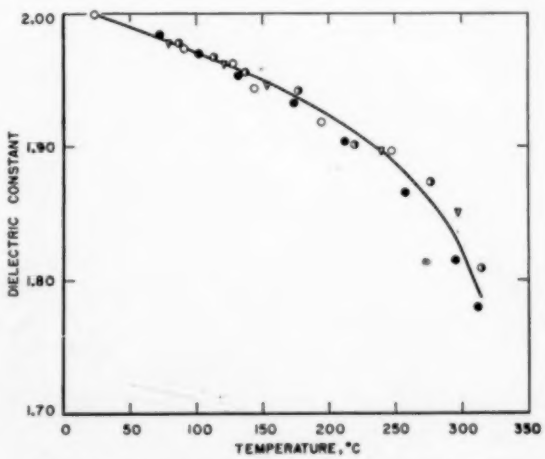

FIGURE 2. *Dielectric constant of Teflon at any frequency between 10^2 and 10^5 c/s as a function of temperature.*

◑, sample A; ○, sample B; ▽, sample C; ●, sample D.

dissipation factor are of the order of 10^{-4}. No satisfactory data on nonpolar polymers with losses of that order of magnitude have as yet been published, and theories [6, 7] put forward to explain the nature of such losses have therefore remained untested.

Quantitative information on phase transitions in Teflon is available both on the basis of dilatometric [8] and of thermodynamic measurements [9]. These investigations agree as to the occurrence in the room-temperature range of a double first-order transition, both steps of which presumably occur between crystalline forms, the less pronounced step occurring at about 30° C, whereas the one involving the larger volume change occurs at about 20° C. The volume changes associated with this transition were not indicated by the thickness measurements made on the sample in the holder because these measurements were very crude compared to dilatometric measurements. The fact that there appears to be no drastic change in dielectric constant in this region does not appear surprising if one assumes that the transition occurs between essentially nonpolar crystals. The high-temperature melting transition at 327° C can be easily indicated by the dielectric measurements as it is associated with dimensional changes of sufficient magnitude to result in large capacitance changes. There was considerable warping of the sample at this temperature, and attempts to carry out reproducible measurements through this transition range were abandoned.

5. Summary

The variation of the dielectric properties of Teflon from 24° to 314° C can be accounted for in terms of the variation of the bulk density of a nonpolar material.

The author expresses his appreciation to A. H. Scott for helpful advice throughout this investigation.

6. References

[1] W. E. Hanford and R. M. Joyce, J. Am. Chem. Soc. **68**, 2082 (1946).

[2] A. H. Scott, P. Ehrlich, and J. F. Richardson, in preparation; also, Annual report of conference on electrical insulation (1953).

[3] P. Ehrlich and N. J. DeLollis, J. Research NBS **51**, (1953) RP2444.

[4] P. Ehrlich, J. Research NBS **50**, 19 (1953) RP2382.

[5] M. Gevers and F. K. DuPre, Trans. Faraday Soc. **42A**, 47 (1946).

[6] L. E. Sutton, Trans. Faraday Soc. **42A**, 170 (1946).

[7] C. G. Garton, Trans. Faraday Soc. **42A**, 56 (1946).

[8] F. A. Quinn, D. E. Roberts, and R. N. Work, J. Applied Phys. **22**, 1085 (1951).

[9] G. T. Furukawa, R. E. McCoskey, and G. J. King, J. Research NBS **49**, 273 (1952) RP2364.

WASHINGTON, August 1953.

Journal of Research of the National Bureau of Standards Vol. 51, No. 4, October 1953 Research Paper 2450

pH of Solutions of Potassium Tetroxalate from 0° to 60° C

Vincent E. Bower, Roger G. Bates, and Edgar R. Smith

The National Bureau of Standards conventional activity scale of pH is defined in terms of a series of standard buffer solutions prepared from certified materials issued as NBS Standard Samples. In order to increase the accuracy of measurements at low and high pH, standards of high acidity and high alkalinity are needed to supplement the four now available, which cover adequately the intermediate range from 3.5 to 9.2.

Potassium tetroxalate dihydrate, chosen as the fifth pH standard, is a stable, crystalline substance composed, in addition to water, of equal molar amounts of oxalic acid and potassium acid oxalate. Its solutions are therefore well buffered in the concentration range 0.01 to 0.1 M and are highly acidic, with pH ranging from 1.5 to 2.2. Electromotive-force data were obtained for 12 mixtures of potassium tetroxalate and potassium chloride at 13 temperatures from 0° to 60° C, and pH values were assigned to 0.1-, 0.05-, 0.025-, and 0.01-M solutions of potassium tetroxalate without added chloride. The 0.05-M solution, which has a pH value of 1.68 from 15° to 35° C, is recommended as a standard for measurements at low pH.

1. Introduction

There are two primary reasons for the establishment of pH standards. The first and more important is to provide a reference for the adjustment of all pH equipment to a common basis, making possible true reproducibility of pH measurements from time to time and from place to place. The second purpose of pH standardization is to simplify the interpretation of the measured pH and to make it uniform over the entire range of the scale.

The first of these objectives can be met by the universal adoption of a single pH standard. The second is not so easily achieved. The unknown and variable potential at the liquid junction, indicated by the vertical line, in the practical pH cell

$$\text{Pt; } H_2 \text{ (or glass electrode), solution } X \mid \text{3.5 } M \text{ or saturated KCl, } Hg_2Cl_2\text{; Hg} \qquad (1)$$

makes the interpretation of measured pH values in terms of concentrations or activities very difficult. Indeed, it is justifiable to assume that the practical pH lies on the scale defined by the standards only when solution X is a dilute aqueous solution of simple ionized solutes.

As is well known, the liquid-junction potential results from transfer of the positive and negative ions across the boundary in unequal numbers. Inasmuch as the transference numbers of all the ions are different, and possibly also the concentration gradients of the several ions through the boundary, the net charge transferred is rarely zero. It is impossible to make an exact correction for the variable liquid-junction potential. Hence, an unchanged liquid, junction potential on substitution of the standard (S) for the unknown solution in the cell is implied in the operational definition of the practical pH value:

$$\text{pH} = \text{pH}_S + \frac{(E - E_S)F}{RT \ln 10}. \qquad (2)$$

In eq (2), E and E_S represent the electromotive force of cell 1 when the unknown and the standard solution (whose pH is pH_S), respectively, are in contact with the electrodes.

The hydrogen and hydroxyl ions have much greater mobilities than other ions. Furthermore, the mobilities of these other ions are all of the same order. For this reason, the liquid-junction potentials depart appreciably below pH 3 and above pH 11 from the relatively constant values maintained in the region of intermediate pH. At high acidities and high alkalinities, therefore, the measured pH may not be susceptible to the same simple interpretation given it near pH 7. When measurements below pH 3 and above pH 11 are to be made, this defect can be remedied to some degree by the choice of standards that are themselves highly acidic or highly alkaline [1][1].

To permit as far as possible a consistent interpretation of the pH over the entire scale, the National Bureau of Standards is establishing a series of standards extending from low to high pH. The standard pH is based upon emf measurements of cells free from a liquid junction and its attendant uncertainties. The standard pH scale is thus defined in terms of several fixed points in much the same manner as the International Temperature Scale.

The pH of the standards is defined formally by

$$\text{pH}_S \equiv -\log a_H, \qquad (3)$$

where a_H is a conventional hydrogen-ion activity. Also by definition, $a_H \equiv f_H m_H$, in which f_H and m_H are the activity coefficient and molality of hydrogen ion. Inasmuch as the activity coefficient of a single ionic species cannot be determined, the numerical values of pH_S must have a conventional or defined basis. The NBS pH values rest upon the average of several reasonable estimates of the individual activity coefficient. At ionic strengths less than 0.1, the pH_S

[1] Figures in brackets indicate the literature references at the end of this paper.

values computed in these several ways are the same within about ± 0.01 unit [2, 3, 4].

Potassium tetroxalate dihydrate, a stable acid salt, is a promising standard for the acid region. Its aqueous solutions, formed by weighing a single solid substance, contain equal molar amounts of oxalic acid and potassium binoxalate and are therefore well buffered. The pH is of the same order of magnitude as $-\log K_1$, where K_1 is the first dissociation constant of oxalic acid. This acid group is moderately strong, with $K_1=0.0536$ at 25°, according to Darken [5]; hence, solutions of potassium tetroxalate with pH less than 2 can be prepared.

2. Method

The method by which the standard pH values (pH_S) were assigned to solutions of potassium tetroxalate has been described earlier.[2] There are three steps in the procedure. First, the emf, E, of cells of the type

$$\text{Pt; } H_2 \text{ (g, 1 atm), K tetroxalate } (m_1), \text{ KCl } (m_2), \text{ AgCl; Ag} \qquad (4)$$

was measured and, with a knowledge of m_2, the molality of chloride ion in the buffer solution, values of the quantity pwH calculated by the equation

$$\text{pwH} \equiv -\log (f_H f_{Cl} m_H) = (E-E^\circ)F/(2.3026RT) + \log m_2, \qquad (5)$$

where E° is the standard potential of cell 4 and the other symbols have their usual significance.[3]

The second step was to determine pwH°, the limit approached by pwH for each buffer solution as the molality of added chloride was reduced. This was accomplished by the determination of pwH for chloride molalities of 0.015, 0.01, and 0.005, plotting pwH as a function of m_{Cl} (that is, m_2), and extrapolating to $m_{Cl}=0$.

The third step was to compute pH_S from pwH°. From the definitions of pH_S and pwH, we have

$$pH_S = \text{pwH}^\circ + \log f^\circ_{Cl}, \qquad (6)$$

where f°_{Cl} is the limit approached by the activity coefficient of chloride ion as the composition of the buffer-chloride mixture approaches that of the pure buffer solution. A nonthermodynamic assumption must be introduced at this point to permit the ionic activity coefficient to be evaluated.

The several reasonable conventional definitions of this coefficient that have been employed earlier for the computation of pH_S [6, 10, 11, 12] are all consistent with the Debye-Hückel equation

$$-\log f^\circ_{Cl} = \frac{A\sqrt{\mu}}{1+Ba_i\sqrt{\mu}} \qquad (7)$$

in which μ is the ionic strength, a_i is the ion-size parameter, and A and B are constants for aqueous solutions at a particular temperature.[4] These assumptions differ essentially only in the value of a_i and the manner in which this value was chosen. By combination of eqs (6) and (7),

$$pH_S = \text{pwH}^\circ - A\sqrt{\mu}/(1+Ba_i\sqrt{\mu}). \qquad (8)$$

From an examination of the mean activity coefficients of hydrochloric acid and chloride salts, it may be concluded that a_i for chloride ion probably lies between 3 and 6. When the concentration of the tetroxalate is 0.05 M, this uncertainty (± 1.5) in a_i amounts to less than 0.01 unit in the assigned pH_S.

3. Experimental Procedures and Results

The potassium tetroxalate dihydrate ($KH_3(C_2O_4)_2{\cdot}2H_2O$) was a composite sample of a 250-lb lot purchased for issuance as NBS Standard Sample 189. The material was slightly moist. Before it was dried it was found to assay 99.6 to 99.7 percent by titration with a carbonate-free 0.17-M solution of sodium hydroxide to the endpoint of phenolphthalein. After drying three samples for 2 to 3 hours in air at 50° C, they assayed 99.93 ± 0.02 percent. The salt should not be heated above 60° C [1]. The results of other standard tests [14] were as follows:

Chloride: Less than 0.002 percent.
Sodium: Less than 0.02 percent.
Calcium: Less than 0.005 percent.
Iron: Less than 0.001 percent.
Ammonia: Less than 0.002 percent.
Sulfur compounds: None perceptible.
Heavy metals: Less than 0.002 percent (as Pb).
Substances darkening sulfuric acid: None.

The potassium chloride was a bromide-free fused sample prepared in the manner described earlier [15]. The specific conductance of the water used was, on the average, 0.8×10^{-6} ohm^{-1}cm^{-1}. Dissolved air was removed from the solutions by passing nitrogen through them for 2 hours.

Four concentrations of potassium tetroxalate, namely 0.1, 0.05, 0.025, and 0.01 *ml*, were studied. The emf values, corrected in the usual way to a partial pressure of 1 atm of hydrogen, are summarized in table 1. Each recorded figure represents the average for two pairs of electrodes in the same cell. These potentials are in good agreement with similar but less extensive measurements made in an earlier investigation [1].

[2] See, for example, the assignment of pH_S values to solutions of potassium hydrogen tartrate [6].

[3] The values of E° and $2.3026RT/F$ in absolute volts are listed in [7]. The values of the standard potential were derived from the measurements of Harned and Ehlers [8] as recalculated by Hamer, Burton, and Acree [9].

[4] Values of the Debye-Hückel constants from 0° to 100° C will be found in [10]. In the formula for B (bottom of p. 1765), "10^{-9}" should read "10^8".

TABLE 1. *Electromotive-force values for cell 4 from 0° to 60° C.*

KH tetroxalate m_1	Potassium chloride m_2	Electromotive force at (° C.)—												
		0°	5°	10°	15°	20°	25°	30°	35°	40°	45°	50°	55°	60°
0.1	0.015	-------	-------	-------	0.42610	0.42673	0.42740	0.42783	0.42826	0.42860	-------	-------	-------	-------
					-------	-------	.42724	.42779	.42821	.42858	0.42888	0.42908	0.42914	0.42922
					-------	-------	.42732	.42767	.42813	.42852	.42883	.42906	.42911	.42916
	.010	-------	-------	-------	.43616	.43718	.43767	.43905	.43971	.44014	.43959	.44035	.44069	.44088
					.43559	.43654	.43709	.43797	.43888	.43925	.44003	.44044	.44082	.44107
	.005	-------	-------	-------	-------	-------	.43763	.43822	.43884	-------	-------	-------	-------	-------
					.45313	.45407	.45564	.45618	.45719	.45809	.45915	.45986	.46048	.46102
					-------	-------	.45539	.45637	.45728	.45811	.45888	.45971	.46031	.46094
0.05	.015	0.43137	0.43262	0.43377	.43453	.43517	.43598	.43649	.43700	.43740	.43778	.43808	.43826	.43842
		.43133	.43248	.43349	.43438	.43518	.43582	.43646	.43694	-------	.43775	.43803	.43814	.43816
		-------	-------	-------	-------	-------	.43584	.43637	.43654	.43725	.43760	.43779	.43792	.43793
		.44077	.44207	.44325	.44427	.44526	.44620	.44692	.44758	.44817	.44873	.44920	.44957	.44989
		.44077	.44216	.44330	.44435	.44535	.44620	.44697	.44764	.44813	.44870	.44901	.44939	.44935
	.010	.44081	.44209	.44324	.44429	.44529	.44614	.44697	.44760	.44828	.44881	.44923	.44954	.44962
		-------	-------	-------	-------	-------	.44602	.44678	.44736	.44801	.44862	.44905	.44949	.44981
		-------	-------	-------	-------	-------	.44618	.44686	.44753	.44814	.44862	.44897	.44933	.44963
		.45700	.45856	.46003	.46138	.46263	.46398	.46487	.46581	.46667	.46737	.46806	.46870	.46912
	.005	.45703	.45864	.46010	.46149	.46267	.46399	.46497	.46598	.46687	.46757	.46836	.46903	.46961
		-------	-------	-------	-------	-------	.46377	.46494	.46593	.46682	.46764	.46837	.46877	.46937
0.025	.015	.44064	.44193	.44309	.44413	.44524	.44612	.44661	.44728	.44780	.44813	.44840	.44837	.44831
		.44099	.44232	.44348	.44457	.44545	.44629	.44698	.44754	.44797	.44844	.44874	.44899	.44883
		-------	-------	-------	-------	-------	.44602	-------	-------	.44762	-------	.44840	-------	.44867
		.45014	.45162	.45302	.45423	.45532	.45639	.45723	.45800	.45866	.45923	.45974	.46021	.46052
	.010	.45013	.45161	.45302	.45422	.45528	.45635	.45721	.45798	.45871	.45894	.45946	.45986	.46013
		.45024	.45167	.45306	.45430	.45539	.45638	-------	.45776	.45834	.45904	.45953	.45999	.46013
		-------	-------	-------	-------	-------	-------	-------	-------	.45816	-------	.45922	-------	.46007
		.46614	.46814	.46798	.47129	.47271	.47398	.47516	.47627	.47716	.47818	.47897	.47963	.48023
	.005	.46625	.46796	.46962	.47117	.47252	.47389	.47500	.47604	.47704	.47790	.47883	.47952	.48013
		-------	-------	-------	-------	-------	.47378	.47504	.47621	.47718	.47800	.47850	.47925	.47989
		-------	-------	-------	-------	-------	-------	-------	-------	.47657	-------	.47829	-------	.47971
0.010	.015	.45572	.45732	.45870	.45993	.46114	.46243	.46317	.46409	.46481	.46515	.46542	.46572	.46604
		.45550	.45709	.45851	.45966	.46098	.46210	.46275	.46352	-------	-------	-------	-------	-------
		-------	-------	-------	-------	-------	.46237	.46312	.46388	.46468	.46537	.46586	.46626	.46648
		.46494	.46662	.46805	.46952	.47092	.47230	.47368	.47463	.47540	.47628	.47686	.47747	.47785
	.010	.46507	.46684	.46849	.46990	.47121	.47237	.47325	.47408	.47493	.47580	.47636	.47694	.47730
		-------	-------	-------	-------	-------	.47233	.47357	.47444	.47502	.47607	.47675	.47725	.47767
		-------	-------	-------	-------	-------	.47228	.47350	.47434	.47531	.47606	.47681	.47731	.47777
		-------	-------	-------	-------	-------	-------	.47323	.47416	-------	.47568	.47633	.47674	.47716
		.48082	.48292	.48485	.48667	.48838	.48997	.49120	.49243	.49361	.49487	.49577	.49661	.49712
	.005	.48098	.48303	.48490	.48670	.48830	.48975	.49112	.49239	.49355	.49461	.49557	.49639	.49709
		.48097	.48302	.48490	.48664	.48827	.48971	.49117	.49246	-------	.49469	.49563	.49628	.49697

4. Determination of pwH°

The pwH was calculated by eq (5) from each emf value recorded in table 1. In order to obtain pwH°, the value of pwH for each tetroxalate solution in the absence of chloride, two types of extrapolation, illustrated in figure 1, were tried. The pwH values for the 0.1-*m* solution of potassium tetroxalate were first plotted as a function of the molality of chloride. A straight line, the lower line of figure 1, was drawn and extended to zero molality of chloride. The upper line was drawn through the pwH values for solutions containing the three different amounts of chloride but of lower tetroxalate content, so that the three points correspond to a constant ionic strength equal to that of the chloride-free buffer solution. The pwH, obtained by interpolation, is plotted as a function of m_{Cl}/μ, the fractional contribution of the potassium chloride to the ionic strength.

The two types of extrapolation gave the same result, within the error of the determination. Hence, the simpler and more convenient treatment, illustrated by the lower curve, was used. The plots of pwH as a function of the molality of added potassium chloride at 0°, 25°, and 60° C are shown in figures 2, 3, and 4, respectively. The positions of the lines were determined by the method of least squares. The values of pwH° obtained are summarized in table 2. The accuracy of pwH° is judged to be about ±0.003 at 0° and 25° C and ±0.005 at 60° C.

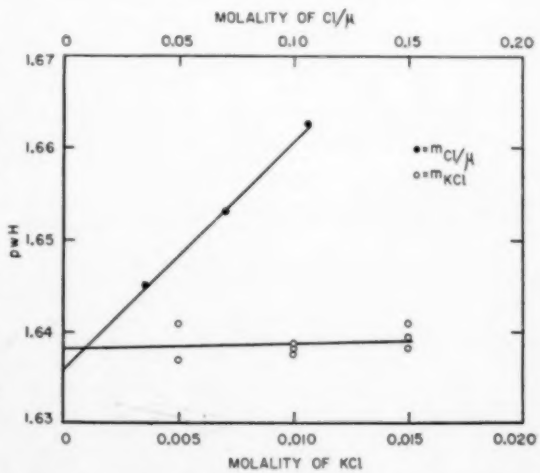

FIGURE 1. *Extrapolation of* pwH *to zero concentration of potassium chloride by two different methods.*

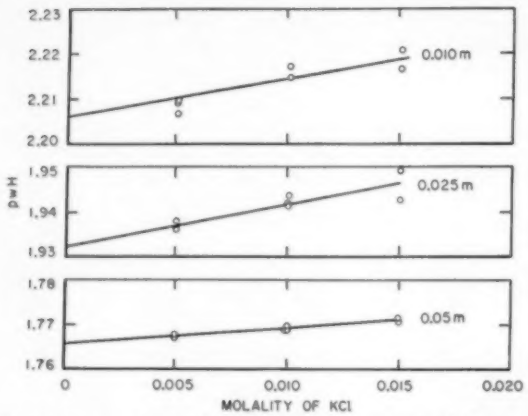

FIGURE 2. pwH *of solutions of potassium tetroxalate as a function of the molality of added potassium chloride at 0° C.*

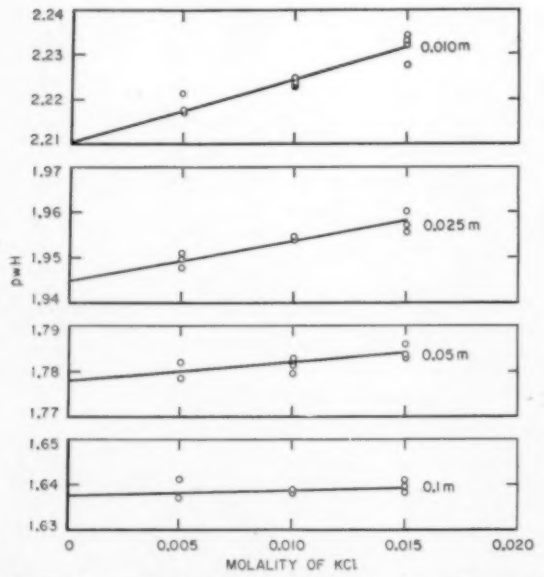

FIGURE 3. pwH *of solutions of potassium tetroxalate as a function of the molality of added potassium chloride at 25° C.*

TABLE 2. pwH° *for four solutions of potassium tetroxalate from 0° to 60°C*

t	0.1 m	0.05 m	0.025 m	0.01 m
°C				
0		1.766	1.933	2.207
5		1.766	1.926	2.204
10		1.765	1.938	2.207
15	1.624	1.770	1.941	2.211
20	1.627	1.773	1.942	2.212
25	1.638	1.778	1.945	2.212
30	1.641	1.783	1.950	2.216
35	1.650	1.791	1.956	2.220
40	1.659	1.796	1.961	2.219
45	1.671	1.804	1.969	2.231
50	1.683	1.813	1.972	2.236
55	1.694	1.821	1.983	2.240
60	1.706	1.828	1.991	2.243

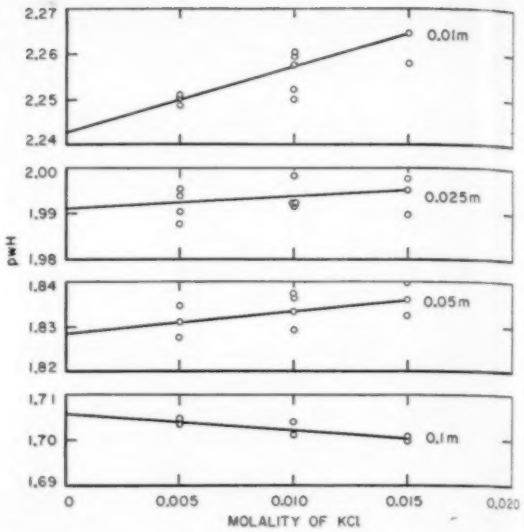

FIGURE 4. pwH *of solutions of potassium tetroxalate as a function of the molality of added potassium chloride at 60° C.*

5. Calculation of pH

The ionic strength of a solution of potassium tetroxalate of molality m_1 is given by

$$\mu = m_1 + m_H. \tag{9}$$

The dissociation of the second acid group of oxalic acid in tetroxalate solutions is so slight that its contribution need not be considered [16]. The hydrogen-ion concentration, m_H, was obtained with sufficient accuracy by the method of successive approximations directly from pwH° with activity coefficients estimated by the Debye-Hückel equation

$$-\log m_H = \text{pwH}^\circ + \log (f_H f_{Cl})^\circ = \text{pwH}^\circ - \frac{2A\sqrt{\mu}}{1+4B\sqrt{\mu}}. \tag{10}$$

The values of the ionic strength at 0°, 25°, and 60° C obtained in this manner are given in table 3.

TABLE 3. *Ionic strengths of four solutions of potassium tetroxalate*

Molality of tetroxalate	Ionic strength at (° C)—		
	0°	25°	60°
0.01	0.0181	0.0180	0.0175
.025	.0417	.0413	.0401
.05	.0772	.0760	.0744
.1	.1433	.1400	.1383

* At 15° C.

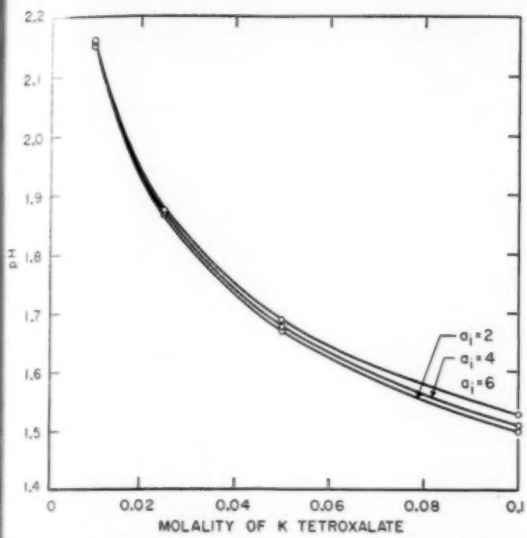

FIGURE 5. pH *of solutions of potassium tetroxalate at 25° C. as a function of molality.*

The three curves represent pH obtained by eq (8), with a_i values of 6, 4, and 2, as marked.

The pH_S at 25°, calculated by eq (8) for three values of a_i, namely, 2, 4, and 6, is plotted in figure 5. The curves converge as the ionic strength decreases. Hence, it is possible, for molalities of tetroxalate not exceeding 0.05, to select an average pH_S that will represent the values on all three curves within ±0.01 unit. Nevertheless, when the mean activity coefficients of hydrochloric acid in its pure aqueous solutions and in solutions with added potassium salts are fitted to equations of type (7), the ion-size parameter is usually found to lie between 4 and 6. For this reason, the pH_S given in table 4 is the average of those computed by eq (8) with a_i=4 and a_i=6. In view of the arbitrary selection of a_i, an uncertainty of ±0.01 is assigned to the values for 0.01-, 0.025-, and 0.05-*M* solutions and ±0.015 to those for the 0.1-*M* solution.

The pH of buffer solutions is not normally very sensitive to changes in the total concentration of buffer substance, although the change of pH upon dilution increases near the ends of the pH scale. It is possible, therefore, to take advantage of the convenience of volumetric methods for the preparation of buffer solutions. It is evident from figure 5 that the pH of tetroxalate solutions at 25° changes about 0.2 unit when the molality drops from 0.05 to 0.025. Two determinations with a 50-ml picnometer showed the density of the 0.05-molal solution to be 1.00320 at 25° C; hence, the 0.05-molal (*m*) solution is 0.0496 molar (*M*). This difference of 0.8 percent in the tetroxalate concentration between 0.05-*m* and 0.05-*M* solutions corresponds to 0.001 to 0.002 pH unit, an entirely negligible amount in comparison with the uncertainty in the assignment of pH_S. It is therefore justifiable to assign the pH_S values determined as described above for 0.01-, 0.025-, 0.05-, and 0.1-*m* solutions also to the solutions of numerically the same molarity, as has been done in table 4.

TABLE 4. pH_S *of four solutions of potassium tetroxalate from 0° to 60° C*

t	0.1 *M*	0.05 *M*	0.025 *M*	0.01 *M*
°*C*				
0	.....	1.671	1.858	2.153
5	.....	1.671	1.860	2.150
10	.....	1.669	1.862	2.152
15	1.508	1.674	1.864	2.156
20	1.509	1.676	1.865	2.156
25	1.520	1.681	1.867	2.156
30	1.521	1.685	1.872	2.160
35	1.530	1.693	1.877	2.162
40	1.538	1.697	1.882	2.162
45	1.549	1.704	1.890	2.174
50	1.560	1.712	1.892	2.179
55	1.570	1.719	1.902	2.182
60	1.580	1.726	1.909	2.185

6. Tetroxalate Buffer Standards

The 0.05-*M* solution is recommended for use as a standard for pH measurements in the acid range.[5] In common with other strongly acidic solutions, it has a high buffer value and a high dilution value. In other words, its pH is little influenced by chance contamination with acid or base but is relatively sensitive, in comparison with buffer solutions of moderate acidity, to dilution or concentration of the buffer components. Nevertheless, the dilution value is not high enough to impair the usefulness of tetroxalate buffer solutions in any significant degree.

The Van Slyke buffer value, β, is defined as the differential ratio $dB/d\text{pH}$ [18] and represents the number of equivalents of strong base (B) required, without volume change, to increase the pH of 1 liter of a particular solution by 1 pH unit. Approximate buffer values are obtained experimentally by measuring the pH change produced by the addition of small volumes of solution, each of which contains ΔB equivalents of concentrated, strong alkali. In this way, the buffer value of 0.05-*M* potassium tetroxalate at 25° C was found to be

$$\frac{dB}{d\text{pH}} \approx \frac{\Delta B}{\Delta\text{pH}} = 0.07. \qquad (11)$$

The pH change was determined with the glass electrode.

The dilution effect is conveniently expressed as the increase of pH on dilution of the buffer solution with an equal volume of pure water. For the 0.05-*M* solution of potassium tetroxalate, this quantity, designated $\Delta\text{pH}_{1/2}$ is

$$\Delta\text{pH}_{1/2} = +0.19. \qquad (12)$$

[5] The assignment of pH_S is least uncertain at low ionic strengths. For this reason, the 0.01-*M* solution was recommended as a pH standard in a preliminary study [17]. The greater reproducibility, stability, and buffer capacity of the 0.5-*M* solution and its lower pH value seem now to justify the selection of this solution.

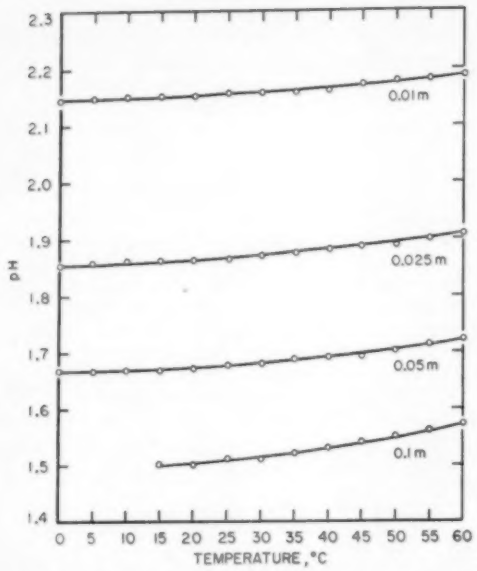

FIGURE 6. pH *of four tetroxalate solutions as a function of temperature.*

The buffer value of the 0.05-*M* solution of potassium acid phthalate is about 0.02, and its dilution value is +0.05; hence, the pH of the tetroxalate solution is altered less than that of the phthalate solution by addition of acid or alkali but is more sensitive to dilution.

As shown in figure 6, the temperature coefficient of pH is small and positive for all four tetroxalate solutions in the range of the measurements. The pH of the 0.05-*M* solution is 1.68±0.01 at all temperatures between 15° and 35° C.

A solution of potassium tetroxalate saturated at at 0° C was used by Schomaker and Brown [19] in their standard quinhydrone half-cell. Hitchcock and Taylor [20] selected the 0.1-*M* solution of this salt as a useful pH standard and assigned to it pH values of 1.480 at 25° and 1.495 at 38° C. These pH values are 0.040 unit lower than those given in table 4, or about two and one-half times the estimated uncertainty of the latter. This difference corresponds to 2.4 mv.

The determination of Hitchcock and Taylor was based on the emf of cells with a liquid junction, and the primary reason for the difference between the values of the two investigations is probably the residual liquid-junction potential, which becomes appreciable at low pH values. In other words, the potential across the boundary between the bridge solution (saturated potassium chloride) and 0.1-*M* potassium tetroxalate differs from that between the bridge and other buffer solutions whose pH values lie closer to neutrality.

Potassium tetroxalate dihydrate can be dried in air at 1-atm pressure at temperatures up to about 60° C without loss of crystal water. The 0.05-*M* solution is prepared by dissolving 12.70 g (air weight) in water and diluting to 1 liter. In an experiment designed to reveal the effect of drying the salt, two solutions were prepared by adding the same weight of wet and dry salt to equal amounts of a solution of potassium chloride. Although the wet sample contained about 0.5 percent of water, the emf of cells prepared from the two solutions displayed no significant differences. Hence, it appears that drying is usually unnecessary. Textroxalate solutions are satisfactorily stable without the addition of preservatives. In order to minimize the effects of evaporation and accidental contamination, however, it is recommended that the standard be replaced every 2 months.

7. References

[1] R. G. Bates, G. D. Pinching, and E. R. Smith, J. Research NBS **45,** 418 (1950) RP2153.
[2] R. G. Bates, Chem. Rev. **42,** 1 (1948).
[3] R. G. Bates and E. R. Smith, J. Wash. Acad. Sci. **38,** (1948).
[4] R. G. Bates, Analyst **77,** 653 (1952).
[5] L. S. Darken, J. Am. Chem. Soc. **63,** 1007 (1941).
[6] R. G. Bates, V. E. Bower, R. G. Miller, and E. R. Smith, J. Research NBS **47,** 433 (1951) RP2268.
[7] R. G. Bates and G. D. Pinching, J. Research NBS **42,** 419 (1949) RP1982.
[8] H. S. Harned and R. W. Ehlers, J. Am. Chem. Soc. **55,** 2179 (1932).
[9] W. J. Hamer, J. O. Burton, and S. F. Acree, J. Research NBS **24,** 269 (1940) RP1284.
[10] R. G. Bates and S. F. Acree, J. Research NBS **34,** 373 (1945) RP1648.
[11] W. J. Hamer, G. D. Pinching, and S. F. Acree, J. Research NBS **36,** 47 (1946) RP1690.
[12] G. G. Manov, N. J. DeLollis, P. W. Lindvall, and S. F. Acree, J. Research NBS **36,** 543 (1946) RP1721.
[13] G. G. Manov, R. G. Bates, W. J. Hamer, and S. F. Acree, J. Am. Chem. Soc. **65,** 1765 (1943).
[14] Chemical reagents, American Chemical Society specifications. American Chemical Society, Washington, D. C. (1950).
[15] G. D. Pinching and R. G. Bates, J. Research NBS **37,** 311 (1946) RP1749.
[16] G. D. Pinching and R. G. Bates, J. Research NBS **40,** 405 (1948) RP1885.
[17] R. G. Bates, G. D. Pinching, and E. R. Smith, J. Research NBS **45,** 418 (1950) RP2153.
[18] D. D. Van Slyke, J. Biol. Chem. **52,** 525 (1922).
[19] V. Schomaker and D. J. Brown, Ind. Eng. Chem., Anal. Ed. **9,** 34 (1937).
[20] D. I. Hitchcock and A. C. Taylor, J. Am. Chem. Soc. **59,** 1812 (1937); **60,** 2710 (1938).

WASHINGTON, July 22, 1953.

Journal of Research of the National Bureau of Standards Vol. 51, No. 4, October 1953 Research Paper 2451

On Small Disturbances of Plane Couette Flow[1]

Wolfgang Wasow[2]

The Orr-Sommerfeld equation for the function $\phi(y)$, which appears in the component $\phi(y)\exp\{i\alpha(x-ct)\}$ of the stream function, is analyzed in detail for the case of plane Couette flow. A set of solutions is found whose asymptotic behavior as $\alpha R\to\infty$ can be calculated in the whole complex y-plane (R is the Reynolds number). A disturbance with given α is proved stable, for any α, if αR is sufficiently large. In addition, an investigation is made of the asymptotic properties of an allied equation for which, in contradistinction to the singular Couette case, an inner friction layer does exist.

1. Introduction

The purpose of this paper is to analyze mathematically some questions connected with the stability of plane Couette flow.

If the space between two infinite parallel planes at constant distance in time is filled with a viscous, incompressible fluid, and if one plane is at rest while the other moves with constant velocity, then the simplest flow compatible with the Navier-Stokes equations and these boundary conditions is the stationary parallel motion with linear velocity profile. This is plane Couette flow. Experiments indicate, [1, p. 185],[3] that this flow, just as most other viscous flows, becomes unstable, that is, turbulent, for high Reynolds numbers.

The oldest and best developed theory of hydrodynamic stability for plane parallel flows, not only for Couette flow, studies the stability of disturbances so small that they can be regarded as solutions of a linearized differential equation. It is further assumed that the stream functions of such disturbances can be obtained by superposition of functions of the form

$$\phi(y)e^{i\alpha(x-ct)}, \tag{1}$$

if the main flow is taken to be parallel to the x-axis. Here, α is positive, c and $\phi(y)$ are complex, and t is the time. The references [1, 2] contain fuller accounts of this theory. It reduces the stability problem to eigenvalue problems for the differential equation

$$\phi^{(4)}-2\alpha^2\phi''+\alpha^4\phi-i\alpha R[(w-c)(\phi''-\alpha^2\phi)-w''\phi]=0, \tag{2}$$

where $w=w(y)$ is the velocity of the main flow and R denotes a Reynolds number of the flow.

A solution (eigenfunction) of (2) that satisfies the homogeneous boundary conditions of a particular flow problem under consideration yields a stable or unstable disturbance of that flow according as the corresponding eigenvalue c has a negative or positive imaginary part. For a given value of R the flow is stable, if one has $\mathrm{Im}\, c\leq 0$ for all possible eigenvalues. Otherwise the flow is unstable.

This approach has been very successful for a number of velocity profiles. It has led to critical Reynolds numbers that are in good agreement with experimental evidence, [4, 5, 6]. A mathematically difficult part of this method is the integration of the differential equation (2). For large values of αR asymptotic methods can be used whose validity has been established in [7, 8 and 10].

Couette flow, however, although it has the simplest velocity profile, plays an exceptional role in these theories. First, the proofs of [7, 8 and 10] do not cover this case. Second, all investigations seem to indicate that Couette flow is stable, in the sense specified above, at all Reynolds numbers, although no mathematically complete proof of this has been given (cf. [2], p. 256). Third, in contrast to other profiles, no so-called "inner friction layers" [3, 8] occur in the theory of Couette flow.

This paper will consist of three parts, corresponding to these three points.

(a) The first part (section 2) is in the nature of a supplement to [9] and [10]. A fundamental system of the differential equation (2) for the case of Couette flow is constructed whose asymptotic behavior, as $\alpha R\to\infty$, can be calculated in the whole complex y-plane.

(b) In the second part (section 3) the eigenvalues c of (2), corresponding to possible disturbances of the flow, are studied as functions of α and αR. It is proved that *for any given α a disturbance of type* (1) *of Couette flow is stable, if αR is sufficiently large.* If the physically plausible conjecture is accepted, that above a certain frequency α there is always stability (cf. [3], part III, p. 284), the stronger statement can be made that, *uniformly in α*, there is a lower bound for αR above which the flow is stable.

On the other hand there are the inequalities of Synge ([2], p. 258), which imply the stability of Couette flow for sufficiently small values of R. Even if taken together, these results do not, of course, constitute a complete mathematical proof of stability. But the author believes that they go farther towards this goal than previous efforts.

C. Morawetz has shown [13] that the possible eigenvalues c of the stability problem fall asymptotically into three classes: (1) Eigenvalues that

[1] The preparation of this paper was sponsored (in part) by the Office of Naval Research, USN.
[2] National Bureau of Standards, Los Angeles, Calif.
[3] Figures in brackets indicate the literature references at the end of this paper.

approach those of the limiting inviscid problem as $\alpha R \to \infty$. The corresponding eigenfunctions approximate those of the inviscid problem except possibly in certain "friction layers." (2) An infinity of eigenvalues lying increasingly close to a certain curve in the c-plane as $\alpha R \to \infty$. They are in no way related to the inviscid differential equation. The corresponding disturbances are always stable. (3) Eigenvalues that approach the points $w(y_1)$ or $w(y_2)$, as $\alpha R \to \infty$, where y_1 and y_2 are the ordinates of the flow boundaries. The actual existence or stability of eigenvalues of this third kind was not discussed in [13].

Since no eigenvalues of the first kind exist for plane Couette flow, its asymptotic stability, in the sense stated above, is proved if the disturbances of the third kind are shown to be stable for sufficiently large values of R. This will be done in section 3.

(c) In all cases examined so far, the actually possible disturbances of laminar flows are approximations to solutions of the inviscid differential equation, except, in general, in certain sectors of the complex y-plane, where they diverge exponentially, as $\alpha R \to \infty$ (cf. [8, 9, 10]). The results of section 2 show that no such sectors of divergence exist in the Couette case.

In section 4, the mathematical reason for this absence is analyzed. Although not immediately applicable to physical problems, the results of that section may turn out to be of more than purely mathematical interest.

2. Solution of the Differential Equation

In terms of the dimensionless quantities used in (2), the velocity profile of Couette flow is, for an appropriate definition of R,

$$w(y) = y. \tag{3}$$

The further substitutions

$$z = y - c, \tag{4}$$

$$\lambda = (-\alpha R i)^{\frac{1}{3}}, \tag{5}$$

$$\phi(y) = u(z) \tag{6}$$

change (2) into the simpler form

$$u^{(4)} - 2\alpha^2 u'' + \alpha^4 u + \lambda^3 z(u'' - \alpha^2 u) = 0. \tag{7}$$

The theory of [10] does not apply to this differential equation, because condition (3.3) of that paper is not satisfied. But (7) can be treated directly by the method of Laplace transformation used in [9].

By a straightforward application of Laplace's method, it is seen that contour integrals of the form

$$u(z,\lambda) = \int_C (t^2 - \alpha^2)^{-1} e^{\lambda^{-2}(t^3/3 - \alpha^2 t) + zt}\, dt \tag{8}$$

are solutions of (7), provided C is a path that is either closed or that extends to infinity in such a way that $Re(\lambda^{-2}t^3) < 0$. Five such paths are indicated in the figure 1, where the sectors in which Re $(\lambda^{-2}t^3) > 0$ have been shaded. The paths $C(A_j)$ $(j=1,2,3)$ are the same as in [9 and 10]. The solutions corresponding to these contours will be called $A_j(z,\lambda)$, $U(z,\lambda)$ and $V(z,\lambda)$. Clearly,

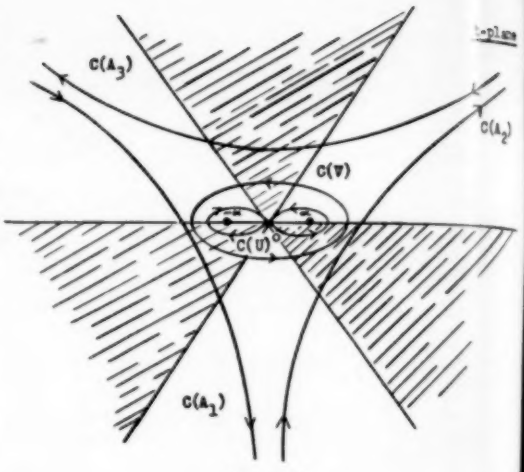

FIGURE 1.

$$A_1 + A_2 + A_3 = V. \tag{9}$$

Let S denote any bounded neighborhood of the origin in the z-plane. Then a short calculation shows that, in S,

$$U(z,\lambda) = \frac{2\pi i}{\alpha} \cosh \alpha z \tag{10}$$

$$V(z,\lambda) = \frac{2\pi i}{\alpha} \sinh, \alpha z. \tag{11}$$

The asymptotic calculation of the solutions $A_j(z,\lambda)$ proceeds exactly as in [9]. It is amply sufficient, therefore, to restate those results.

Let ξ and η be defined by

$$\xi = \frac{2}{3}\lambda(-z)^{3/2}, \quad \eta = \lambda^{2/3} z, \tag{12}$$

and denote by C_k $(k=1,2,3)$ the three rays Re $\xi = 0$ numbered so that

$$\arg z = \frac{4k}{3}\pi - \frac{2}{3}\arg \lambda, \quad \text{on } C_k. \tag{13}$$

The closed sector of S bounded by $C_j, (j \neq k)$, and of central angle $2\pi/3$ may be called S_k. If ξ_0 is any arbitrary positive constant, one has then

(a) For $|\xi| \geq \xi_0$, z in $S - C_k$,

$$A_k(z,\lambda) = \sqrt{\pi}\lambda^{-2/3}\left(\frac{3}{2}\xi\right)^{-5/6} e^{\xi}[1 + O(\xi^{-1})]. \tag{14}$$

Here the determination of ξ for which $\mathrm{Re}\,\xi \leq 0$ in S_k and $\mathrm{Re}\,\xi > 0$ in $S - S_k$ must be taken.

(b) For $|\xi| \leq \xi_0$,

$$A_k(z,\lambda) = \lambda^{-2/3} \int_{C^*(A_k)} t^{-2} e^{t\eta + t^3/3} dt + O(\lambda^{-4/3}), \quad (15)$$

where $C^*(A_k)$ is obtained from $C(A_k)$ by a rotation through $-2/3 \arg \lambda$.

(c) Near C_k the asymptotic behavior of A_k for $|\xi| \geq \xi_0$ follows immediately from (9), (11) and (14).

These asymptotic relations may be indefinitely formally differentiated. Without much additional effort it can be shown that (14) and (15) are first approximations of infinite asymptotic series progressing in powers of ξ^{-1} and $\lambda^{-2/3}$, respectively.

The angle of $\xi^{-5/6}$ in formula (14) is $\pi/2 - 2\pi k/3 \pmod{2\pi}$ at the points of the angular bisector of $S - C_k$. At the other points of the domain $S - C_k$, it is then obtained by analytic continuation. The angle of $\lambda^{-2/3}$ is $-2/3 \arg \lambda$. The angle of λ will be fixed in accordance with (5) by setting

$$\arg \lambda = \frac{3\pi}{4}. \quad (16)$$

3. Stability Problem

The coordinate system and the definition of the Reynolds number can, and will, be chosen so that the boundaries of the flow are at

$$y_1 = 0, \quad y_2 = 1. \quad (17)$$

The boundary conditions for the disturbance are then ([3], p. 134)

$$\phi(0) = \phi(1) = \phi'(0) = \phi'(1) = 0. \quad (18)$$

In terms of the variables introduced in (4), (5) and (6) this becomes

$$u(-c) = u(1-c) = u'(-c) = u'(1-c) = 0. \quad (19)$$

The differential equation (7) with the boundary condition (19) constitutes the eigenvalue problem of plane Couette flow. In view of the results of [13] described in section 1 only those eigenvalues $c = c(\alpha,\lambda)$ need to be studied, for which either

$$\lim_{\lambda \to \infty} c(\alpha,\lambda) = 0, \quad (20)$$

or

$$\lim_{\lambda \to \infty} c(\alpha,\lambda) = 1. \quad (21)$$

(The notation differs from that of [13] in that there $\lambda = \sqrt{\alpha R}$, and that the names of the sectors S_1 and S_2 are interchanged.) The case (20) will be considered first. Using (13) and (16), the sectors S_k are seen to have the appearance indicated by the figure 2.

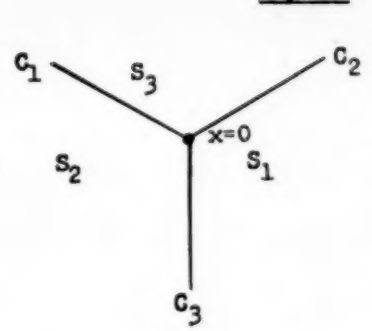

FIGURE 2.

A convenient fundamental system for the present discussion is formed by the functions A_1, A_2, U, V. Then the eigenvalues are the solutions of the equation

$$F(\alpha,c,\lambda) \equiv \begin{vmatrix} A_1(-c) & A_2(-c) & U(-c) & V(-c) \\ A_1'(-c) & A_2'(-c) & U'(-c) & V'(-c) \\ A_1(1-c) & A_2(1-c) & U(1-c) & V(1-c) \\ A_1'(1-c) & A_2'(1-c) & U'(1-c) & V'(1-c) \end{vmatrix} = 0. \quad (22)$$

Two ranges of c have to be distinguished according as $\eta_c = \lambda^{2/3} c$ remains bounded or is unbounded as $\lambda \to \infty$. If η_c is very large, the asymptotic expressions (14) can be used at both end points, and arguments analogous to those employed in [13] show that the corresponding value of c cannot have positive imaginary part.

If η_c remains bounded as $\lambda \to \infty$ the expressions (15) are to be used at $z = 1 - c$ and the expressions (14) for $z = -c$, that is, $\eta = \eta_c$. Setting, for abbreviation

$$g_k(\eta) = \int_{C^*(A_k)} t^{-2} e^{t\eta + t^3/3} dt \quad (23)$$

one finds, after a short calculation, that $F(\alpha,c,\lambda) = 0$ becomes, in this case,

$$g_1'(\eta_c) + \lambda^{-2/3} E(\alpha,\lambda,c,\eta_c) = 0 \quad (24)$$

where $E(\alpha,\lambda,c,\eta_c)$ is bounded for fixed α, as $\lambda \to \infty$, provided η_c remains bounded. Using Rouché's theorem, as in [13], it can be proved that, if $\eta = \eta_0$ is a root of the equation

$$g_1'(\eta) = 0, \quad (25)$$

then

$$\eta_c = \eta_0 + O(\lambda^{-2/3}), \quad (26)$$

that is,

$$c(\alpha,\lambda) = -\lambda^{-2/3} \eta_0 + O(\lambda^{-4/3}). \quad (27)$$

If $c(\alpha,\lambda)\to 1$, the calculations are analogous. The roles of the two end points are interchanged, and A_1 is dominant at the left end point. If η_1 is a root of the equation

$$g_2(\eta)=0, \tag{28}$$

then there exist solutions of $F=0$ of the form

$$c(\alpha,\lambda)=1-\lambda^{-2/3}\eta_1+O(\lambda^{-4/3}). \tag{29}$$

The preceding results reduce the question of the sign of Im c for large Reynolds numbers to inequalities concerning the position of the roots of eq (25) and (28). In order to study this question, it is convenient to introduce the variable

$$s=\omega\eta, \tag{30}$$

where

$$\omega=e^{2\pi i/3}, \tag{31}$$

and the function

$$\psi(s)=\frac{1}{2\pi i}\,g_1'(\eta). \tag{32}$$

Since the definition (23) implies that

$$g_2'(\eta)=g_1'(\omega\eta)=g_3'(\omega^2\eta), \tag{33}$$

all three functions $g_k'(\eta)$ can be simply expressed in terms of $\psi(s)$.

The values $c(\alpha,\lambda)$ given by (27) have, for sufficiently large λ, positive imaginary parts, if, and only if, Re $\eta_0>0$, that is if the zeros of $\psi(s)$ lie in the half-plane $\pi/6<\arg s<7\pi/6$. Similarly, the values $c(\alpha,\lambda)$ given by (29) have, for large λ positive imaginary parts, if Re $\eta_1>0$. From (33) it follows that the necessary and sufficient condition for this to happen is that the zeros of $\psi(s)$ lie in the half-plane $-7\pi/6<\arg s<-\pi/6$. Hence *all disturbances are stable, for sufficiently large Reynolds numbers, if all roots of $\psi(s)$ lie in the sector* $|\arg s|<\pi/6$.

In order to prove that this is indeed the case, a few properties of the function $\psi(s)$ must first be collected.

From (23), (30), (32) and (33), it is seen that the integral representation

$$\psi(s)=\frac{1}{2\pi i}\,g_3'(s)=\frac{1}{2\pi i}\int_{C^*(A_3)} t^{-1}e^{ts+t^3/3}dt \tag{34}$$

is valid. By a calculation very similar to that of $A_3(x,\lambda)$ in [9] asymptotic expressions for $\psi(s)$ can be derived when $|s|$ is large. The calculation results in the following formulas

$$\psi(s)=\begin{cases} \dfrac{1}{2\sqrt{\pi}}\,(-s)^{-3/4}e^{-\frac{2}{3}(-s)^{3/2}}[1+O(s^{-1})] & (35)\\[2ex] 1-\dfrac{1}{\sqrt{\pi}}\,s^{-3/4}\cos\left(\dfrac{2}{3}\,s^{3/2}+\dfrac{\pi}{4}\right) & \\[2ex] \qquad +O\left(s^{-7/4}\exp\left\{\dfrac{2}{3}\,|(\operatorname{Re} s)^{3/2}|\right\}\right). & (36)\end{cases}$$

Here the first formula is valid outside any sector containing the positive real axis, and the second one for $|\arg s|<2\pi/3$. In the common part of these two sectors the two expressions are equivalent. In (35) the powers $(-s)^{-3/4}$ and $2(-s)^{3/2}/3$ are to be taken positive on the negative real axis and continued analytically into the whole sector of validity. In (36) the powers $s^{-3/4}$ and $s^{3/2}$ are positive on the positive real axis and must be continued analytically into $|\arg s|<2\pi/3$. The derivation of (35) and (36) is omitted except for the remark that actually only formula (35) need be proved directly, for from formula (33) one obtains analogous formulas for $g_1'(\eta)$ and $g_2'(\eta)$, and the identity

$$g_1'(\eta)+g_2'(\eta)+g_3'(\eta)=2\pi i, \tag{37}$$

which follows directly from (23), leads then to (36).

Differentiation of the relation (34) shows that

$$\psi'(s)=Ai(-s), \tag{38}$$

where $Ai(s)$ is Airy's integral (cf. [14] and [8]). By (35), the function $\psi(s)$ tends to zero as $s\to\infty$ in the sector $2\pi/3<\arg s<4\pi/3$. Integrating (38) one finds, therefore,

$$\psi(s)=\int_{\Gamma_s} Ai(-t)dt. \tag{39}$$

Where Γ_s is any path starting at infinity in the sector $2\pi/3<\arg t<4\pi/3$ and ending at $t=s$. Since the Airy integral is real for real s, it follows from (39) that $\psi(s)$ is also real on the real axis.

Equations (33) and (37) imply that $\psi(0)=1/3$. Hence, (39) may be replaced by

$$\psi(s)=1/3+\int_0^s Ai(-t)dt. \tag{40}$$

Since Airy's integral is related to Hankel's function by the identity

$$A_i(s)=\frac{\omega}{2\sqrt{3}}\sqrt{s}\,H^{(1)}_{1/3}\left(\frac{2i}{3}\,s^{3/2}\right),$$

where the branch of the three-valued Hankel function is determined by the condition that $Ai(s)$ must be real on the real axis, the integral in (39) can be transformed into

$$\psi(s)=\frac{\omega}{2i\sqrt{3}}\int_{L_\zeta} H^{(1)}_{1/3}(\tau)d\tau. \tag{41}$$

Here

$$\zeta=\frac{2}{3}\,i(-s)^{3/2}, \tag{42}$$

and L_ζ is a path that begins at $\tau=\zeta$ and goes to infinity in the upper half plane. As the function $H^{(1)}_{1/3}(\tau)$ has a branch point at $\tau=0$, while $\psi(s)$ is single valued, the position of L_ζ with respect to the origin must be specified. If

$$0\le\arg s<\pi, \tag{43}$$

and the determination of ζ in (42) is taken for which

$$-\pi<\arg\zeta\leq\frac{\pi}{2}, \tag{44}$$

a short argument, omitted here, shows that L_ζ must be in $-\pi<\arg\tau<\pi/2$.

As to the zeros of $\psi(s)$, it follows from the asymptotic representation (35) that outside a sufficiently large circle they must all lie arbitrarily close to the positive real axis.

On the other hand, $\psi(s)$ *has no real zeros.* To show this, one can use the fact that $\psi(s)$ is a solution of the differential equation

$$\psi'''+s\psi'=0. \tag{45}$$

This can be verified, either by means of (34), or by using (39) and the differential equation for Airy's function. If (45) is multiplied by 2ψ, the relation

$$\frac{d}{ds}(2\psi''\psi-\psi'^2)+s\frac{d}{ds}(\psi^2)=0 \tag{46}$$

is obtained. Assume, now, that $s=a$ is a zero of $\psi(s)$. Integrating (46) from $-\infty$ to a, it follows then that

$$\psi'^2(a)+\int_{-\infty}^{a}\psi^2(t)dt=0.$$

This is impossible for real a, because $\psi(s)$ is real on the real axis.

After these preparations, it will now be proved that the sector $\pi/6\leq\arg s\leq 11/6\pi$ contains no zeros of $\psi(s)$. Since $\psi(s)$ assumes conjugate values at conjugate points, only the sector $\pi/6\leq\arg s\leq\pi$ needs to be investigated.

Consider first the portion of this sector for which

$$|s|\geq r_0. \tag{47}$$

If r_0 is chosen so large that the remainder denoted by $O(s^{-1})$ in formula (35) is numerically less than unity, for $|s|\geq r_0$, the absence of zeros of $\psi(s)$ in the domain under consideration is a direct consequence of Rouché's theorem. An appraisal of the remainder can be based on the following lemma, which is a special case of a more general result of Weber [16, 17, p. 212].

LEMMA 1. *If $R(s)$ is defined by*

$$H^{(2)}_{1/3}(s)=\left(\frac{2}{\pi s}\right)^{\frac{1}{2}}e^{i(s-5\pi/12)}[1+R(s)], \tag{48}$$

then

$$|R(s)|\leq\frac{5\pi}{72}\left|1-\frac{11}{12|s|}\right|^{-17/3}\left(1+\frac{8}{3|s|}\right)^2|s|^{-1} \tag{49}$$

for $-\pi<\arg s<2\pi$.

Substitution of (48) into (41) followed by an integration by parts leads to the expression

$$\psi(s)=\frac{e^{-i\pi/4}}{\sqrt{6\pi}}\left[\zeta^{-1/2}e^{i\zeta}-\int_{L_\zeta}\tau^{-3/2}e^{i\tau}\left(\frac{1}{2}+iR(\tau)\tau\right)d\tau\right]. \tag{50}$$

From (42), (44) and (47) it follows that ζ lies in the sector $-5\pi/4\leq\arg\zeta\leq 0$ of the τ-plane at a distance from the origin not less than $|\tau|=2r_0^{3/2}/3$. The path L_ζ may be chosen as the ray

$$\tau=\zeta+\rho e^{i\pi/8}.$$

Then

$$\left|\int_{L_\zeta}\tau^{-3/2}e^{i\tau}\left(\frac{1}{2}+iR(\tau)\tau\right)d\tau\right|$$

$$\leq\left|\zeta^{-3/2}e^{i\zeta}\right|\int_{L_\zeta}|(\zeta/\tau)^{3/2}e^{i(\tau-\zeta)}|\left(\frac{1}{2}+|R(\tau)\tau|\right)|d\tau|$$

$$\leq|\zeta^{-1/2}e^{i\zeta}|\cdot\frac{3}{2}r_0^{-3/2}\left(\sin\frac{\pi}{8}\right)^{-5/2}\left(\frac{1}{2}+|R(\tau^*)\tau^*|\right), \tag{51}$$

where

$$\tau^*=\frac{2}{3}r_0^{3/2}\sin\frac{\pi}{8}.$$

For $r_0=9$, the expression (51) turns out to be less than $(0.89)|\zeta^{-1/2}e^{i\zeta}|$.

Reinsertion into (50) shows that the quantity $O(s^{-1})$ in (35) is indeed numerically less than one—even less than 0.89—for $\pi/6\leq\arg s\leq\pi, |s|\geq 9$. There are therefore no zeros of $\psi(s)$ in this region. For $|s|\leq r_0$ the following extension of Rouché's theorem is needed.

LEMMA 2. *Let $\psi(z)$ be regular analytic in the simply connected open region G. Let $f(z)$ be defined and piecewise continuous on the rectifiable Jordan curve C in G. Assume that on C*

$$|\psi(z)-f(z)|<|f(z)|. \tag{52}$$

Denote by $\Delta\arg f$ the total change of $\arg f(z)$ as C is once described in positive direction. Then the number of zeros of $\psi(z)$ inside C is the integer nearest $\Delta\arg f/2\pi$. Here $\arg f(z)$ can—and must—be defined so that it changes continuously at points of continuity of $f(z)$ and that it jumps by less than π at the discontinuities of $f(z)$.

PROOF: The inequality (52) excludes the possibility of $\psi(z)$ having a zero on C. Let C be defined by the equation $z=h(t)$, $0\leq t<1$. Define $\alpha(t)$ as a continuous function such that

$$\alpha(t)=\arg\psi(h(t)),\quad 0\leq t<1.$$

Without loss of generality $f(h(t))$ can be supposed continuous at $t=0$. Because of (52),

$$\mathrm{Re}\left(1+\frac{\psi-f}{f}\right)>0.$$

27-200—53——3

Hence,

$$\left|\alpha(t)-\arg f(h(t))\right|=\left|\arg\left(1+\frac{\psi-f}{f}\right)\right|<\frac{\pi}{2},\quad (0\leq t<1)$$

for a certain uniquely defined determination of $\arg f(h(t))$. Let this determination be called $a(t)$. The last inequality implies that $a(t)$ is continuous, except for possible jumps of less than π at the discontinuities of $f(h(t))$, and that

$$|[a(t)-a(0)]-[\alpha(t)-\alpha(0)]|<\pi.$$

Since the exact number of roots of ψ inside C is $[\alpha(t)-\alpha(0)]/2\pi$, the lemma is proved.

This lemma will be applied to a contour Γ in the s-plane consisting of three arcs Γ_1, Γ_2, Γ_3 as follows: Γ_1 is the segment from $s=0$ to $|s|=9$ on the ray $\arg s=\pi/6$; Γ_2 is the circular arc defined by $s=9e^{i\theta}$, $\pi/6\leq\theta\leq\pi$, and Γ_3 is the segment on the real s-axis between $s=-9$ and $s=0$. On Γ_1, the function $f(s)$ is to be an appropriate partial sum of the ascending power series for $\psi(s)$. On Γ_2, the leading term of the asymptotic series for $\psi(s)$ can be taken as $f(s)$. On Γ_3, the function $f(s)$ is identical with $\psi(s)$.

The ascending series for $\psi(s)$ follows from (40) by termwise integration of the series for $Ai(-t)$, see [15] p. B17). Separation of the real and imaginary parts for $\arg s=\pi/6$ produces then two series with real terms of alternating sign and decreasing moduli, at least from a certain term onward. This fact makes it easy to find the number of terms needed on this ray for $f(s)$ to satisfy the inequality (52).

The necessary calculations were first carried out at the National Physical Laboratory, Teddington (England) under the direction of F. W. Olver. In this calculation r_0 was taken equal to 10, and 13 terms of the series were needed to obtain $\arg f(s)$ to two decimals of a radian on Γ_1.

Equivalent computations were then performed, by a somewhat different method, at the Institute for Numerical Analysis of the National Bureau of Standards, under the direction of G. Blanch. For $|s|\leq 6$ the values of $f(s)$ on Γ_1 were obtained by numerical integration from tables of the Harvard Computation Laboratory [18]. For $6\leq|s|\leq 9$ the procedure was the same as Olver's. These computations show that the contribution $\Delta_1 \arg f$ of Γ_1 to the total change $\Delta \arg f$ of the argument of $f(s)$ is -3.42π. On his longer ray Olver obtained the value of -4.11π radians.

On Γ_2 the inequality (52) is satisfied by virtue of the appraisal of the remainder used for $|s|\geq 9$. The contribution $\Delta_2 \arg f$ of Γ_2 to $\Delta \arg f$ is

$$\Delta_2 \arg f=-\frac{5}{8}\pi+\frac{\sqrt{2}}{3}9^{3/2}=3.43\pi.$$

The corresponding value for $|s|=10$ is 4.12π.

Finally, the contribution $\Delta_3 \arg f$ is zero, because $\psi(s)$ is real on the real axis. The condition (52) is here satisfied, since $\psi(s)$ was proved to have no zeros on the real axis.

Summarizing, it is seen that $\Delta f=0.01\pi$ on the contour formed with the arc $|s|=9$ as well as on the contour with arc $|s|=10$ used by Olver. Reference to lemma 2 then completes the proof that $\psi(s)$ has no zeros in the sector $\pi/6\leq\arg s\leq 11/6\pi$.

The author expresses his thanks for the advice and help he received from Dr. Olver and from Dr. Blanch in this section of the paper.

4. The Differential Equation $u^{(4)}+\lambda^2 z(u''+u)=0$

The occurrence of an inner friction layer is frequently regarded as a mathematical consequence of the fact that the inviscid equation is singular at the point where $w(y)-c=0$. In the case of plane Couette flow the inviscid equation, $\phi''-\alpha^2\phi=0$ is regular at that point, and it seems plausible that this fact is responsible for the absence of an inner friction layer implied by the unrestricted validity of formulas (10) and (11). It will, however, be shown in this section that this view is not quite correct. The total absence of an inner friction layer is actually a very special feature of the differential equation (7). This will become apparent from the discussion below, of the differential equation

$$u^{(4)}+\lambda^2 z(u''+u)=0. \tag{53}$$

The reduced equation $u''+u=0$ corresponding to that differential equation is also regular in the whole finite plane. But even a qualitative a priori argument shows that some form of an inner friction layer is to be expected. The solutions of (53) are all regular at $z=0$, and their fourth derivatives must therefore vanish there. The reduced equation $u''+u=0$ has, however, only one linearly independent solution with this property. No solution $u(z,\lambda)$ of the full equation can, therefore, have a fourth derivative that converges to the fourth derivative of, say, $\cos z$ in a full neighborhood of $z=0$. But then $u(z,\lambda)$ cannot even converge uniformly on any circle $|z|=\text{const}$, as $\lambda\to\infty$, for $u(z,\lambda)$ is an analytic function of z inside the circle and it would follow that $u^{(4)}(z,\lambda)$ converges uniformly in a neighborhood of $z=0$, which is a contradiction. This remark will now be confirmed and amplified by actually solving the differential equation (53).

The usual technique of integration by Laplace contour integrals leads here to solutions of (53) of the form

$$u(z,\lambda)=\int_C (i-t)^{\epsilon-1}(i+t)^{-\epsilon-1}e^{zt+\lambda^{-2}(t^3/3-t)}\,dt, \tag{54}$$

where

$$\epsilon=1/2i\lambda^2. \tag{55}$$

Here C must be a contour such that the integral exists, and that the contributions from the boundary occurring in the calculations leading to (54) vanish.

The discussion of these paths in this example is made complicated by the fact that the integrand has

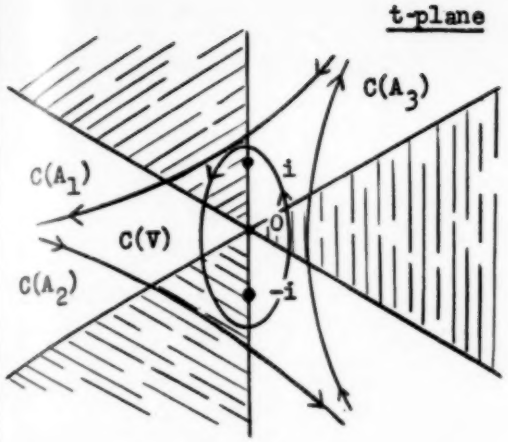

FIGURE 3.

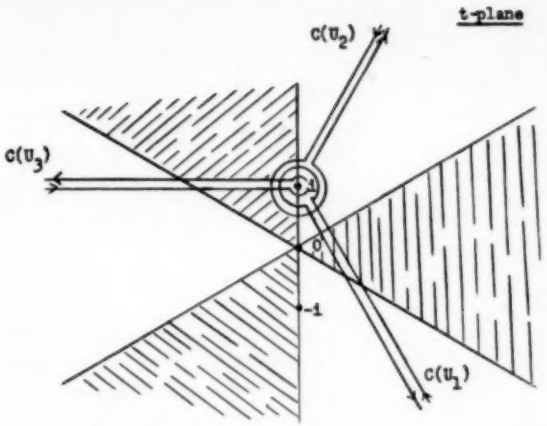

FIGURE 4.

branch points at $t=\pm i$. In order to bring out the analogy with the investigations in [9] seven paths are introduced, which are illustrated in the figures 3 and 4 under the assumption that $\lambda>0$.

As to the determination of the multivalued integrand to be taken the following stipulations are made: (1) Two points of the Riemann surface of the integrand are considered to be on the same sheet, if they can be joined by an arc on the Riemann surface that does not cross the segment connecting the points $t=-i$ and $t=i$. (2) $C(V)$; $C(A_k)$, $(k=1,2,3)$, the lower edge of $C(U_3)$, the upper edge of $C(U_2)$, and the right edge of $C(U_1)$ lie in the same sheet.

As before, the functions defined by (54) will be called A_k, U_k, V according as C is taken to be $C(A_k)$, $C(U_k)$ or $C(V)$, respectively.

From these definitions the following identities can be derived:

$$A_1+A_2+A_3=V, \tag{56}$$

$$U_2-U_2=(e^{\pi\lambda^2}-1)A_1, \tag{57}$$

$$U_2-U_1=(e^{\pi\lambda^2}-1)A_3. \tag{58}$$

They result directly from an inspection of the paths concerned and the fact that the integrand in (54) is multiplied by $e^{\pi\lambda^2}$, if the point $t=i$ is circled once in positive direction. The further identity

$$U_3-U_1=(e^{\pi\lambda^2}-1)(V-A_2) \tag{59}$$

follows by a linear combination of the preceding ones.

The asymptotic calculation of the $A_k(z,\lambda)$ for large λ differs only in trivial details from these given in [9], and the results are exactly the same.

For $V(x,\lambda)$ one finds without difficulty the asymptotic expression

$$V(z,\lambda)=\int_{C(V)}(1+t^2)^{-1}e^{tz}dt+O(\lambda^{-2})$$
$$=2\pi i\sin z+O(\lambda^{-2}), \tag{60}$$

valid in any bounded domain.

For the asymptotic calculation of U_k for z in $S-S_k$ and $|\xi|\geq\xi_0>0$, one can proceed essentially as in [10], p. 12. Since

$$\int_{C(U_k)}\frac{t^m}{1+t^2}e^{tz}dt=\frac{d^m}{dz^m}(\pi e^{tz}),$$

one has

$$\frac{d^m}{dz^m}\{U_k-\pi e^{tz}\}$$
$$=\int_{C(U_k)}[(t-i)^{\epsilon-1}(t+i)^{-\epsilon-1}e^{\lambda^2(t^3/3-t)}-(1+t^2)^{-1}]t^me^{tz}dt$$
$$=\int_{C(U_k)}[e^{\lambda^2(t^3/3-t+\arctan t)}-1]\frac{t^m}{1+t^2}e^{tz}dt. \tag{61}$$

The expression in brackets in the last integral is numerically less than a constant multiple of $|\lambda^{-2}(t^3/3-t+\arctan t)|\max_{t\in C(U_k)}e^{\mathrm{Re}\,[\lambda^2(t^3/3-t+\arctan t)]}$, hence the integral is of the form

$$\lambda^{-2}\int_{C(U_k)}t^{m+1}e^{tz}f(t,\lambda)dt,$$

where $f(t,\lambda)$ is uniformly bounded on $C(U_k)$. Split $C(U_k)$ into a circle C_1 of radius r about $t=i$ and two rays C_2 and C_3 going to, and coming from, infinity

at the same angle, in two different sheets of the Riemann surface. The contribution of C_1 to the integral is $O(\lambda^{-2})$. The contributions of C_2 and C_3 differ only by the factor $-e^{\pi/\lambda^2}$. Hence their sum is

$$(e^{\pi/\lambda^2}-1)\int_{C_2} t^{m+1}e^{tz}f(t,z)dt.$$

By means of the transformation $\tau=tz$, the value of this integral is found, similarly as in [10], p. 13, to be $O(\lambda^{-4}z^{-m-2})=O(\lambda^{2(m+2)/3-4}\xi^{-2(m+2)/3})$. Hence,

$$U_k^{(m)}(z,\lambda)=\frac{d^m}{dx^m}(\pi e^{tz})+O(\lambda^{-2})+O(\lambda^{2(m+2)/3-4}\xi^{-2(m+2)/3}), \tag{62}$$

for z in $S-S_k$ and $|\xi|\geq\xi_0>0, m\geq 0$. The remainder in (62) is $O(\lambda^{-2})$ for all m, if z is bounded away from zero. Otherwise, the remainder tends to zero for $m\leq 4$, but not necessarily for $m>4$.

In order to deal with the higher derivatives and also with the case $|\xi|\leq\xi_0$, observe that the contribution to (54) from the path C_1 is in any case equal to

$$\frac{d^m}{dx^m}(\pi e^{tz})+O(\lambda^{-2}).$$

The contribution of the two rays C_2 and C_3 is, if σ is defined by $\lambda^{-2}t^3=\sigma^3$,

$$(e^{\pi/\lambda^2}-1)\lambda^{2(m-1)/3}\int_{C_2^*}\exp\{\sigma^3/3-$$

$$\lambda^{-4/3}\sigma+\lambda^{-2}\arctan\sigma\,\lambda^{2/3}+\eta\sigma\}\frac{\sigma^m}{\lambda^{-4/3}+\sigma^2}\,d\sigma,$$

and a short argument, omitted here, shows that this is equal to

$$\lambda^{2(m-1)/3-2}\int_{C_2^*}e^{\sigma^3/3+\eta\sigma}\sigma^{m-2}d\sigma\,[1+O(\lambda^{-2/3})],$$

where C_2^* is a ray in the σ-plane along which $\mathrm{Re}\,\sigma^3<0$ and whose initial point has at least the distance $|\lambda^{-2/5}|$ from the origin.

In S_k, finally, the asymptotic behavior of $U_k(z,\lambda)$ follows immediately from the identities (57) to (59), the asymptotic properties of the $A_k(z,\lambda)$, and (62). It is then seen that $U_k(z,\lambda)$ diverges for $|\xi|\geq\xi_0$ in the whole interior of S_k in the same fashion as the corresponding functions in [9] and [10], except for a factor $e^{\pi/\lambda^2}-1=O(\lambda^{-2})$.

Thus, there is in this problem an "inner friction layer" of finite thickness for $|\xi|\geq\xi_0$, and also a friction layer at $z=0$. The latter occurs only in the derivatives of order four or higher.

5. References

[1] L. Prandtl, The mechanics of viscous fluids, Aerodynamic theory, **III,** Reprint edition (Calif. Inst. of Tech., Pasadena, Calif., 1943).

[2] J. L. Synge, Hydrodynamic stability, Semicentennial publications of the Am. Math. Soc. **2,** 227–269 (1938).

[3] C. C. Lin, On the stability of two-dimensional parallel flows, Quart. Appl. Math. **3,** 117–142, 218–234, 277–301 (1945).

[4] W. Tollmien, Laminare Grenzschichten, Hydro- and aerodynamics, Fiat review of German science 1939–1946 (Wiesbaden, 1948).

[5] G. B. Schubauer and H. K. Skramstadt, Laminar boundary-layer oscillations and stability of laminar flow, J. Aeronaut. Sci. **14,** 69 (1947).

[6] H. L. Dryden, Recent advances in the mechanics of boundary-layer flow, Advances in applied mechanics I (New York, N. Y., 1948).

[7] W. Tollmien, Asymptotische Integration der Stoerungsdifferentialgleichung ebener laminarer Strönungen bei hohen Reynoldschen Zahlen, Z. Angew. Math. Mech. **25,** 33–50; **27,** 70–83 (1947).

[8] W. Wasow, The complex asymptotic theory of a fourth order differential equation of hydrodynamics, Ann. Math. **49,** 852–871 (1948).

[9] W. Wasow, A study of the solution of the differential equation $y^{(6)}+\lambda^2(xy''+y)=0$ for large values of λ, Ann. Math. **52,** 350–361 (1950).

[10] W. Wasow, Asymptotic solution of the differential equation of hydrodynamic stability in a domain containing a transition point, Ann. Math. (to be published).

[11] Lord Rayleigh, Further remarks on the stability of viscous fluid motion, Sci. Pap. **VI,** 341–349 (Cambridge, 1920).

[12] C. L. Pekeris, On the stability problem in hydrodynamics, Proc. Cambridge Phil. Soc. **32,** 55–66 (1936).

[13] C. S. Morawetz, The eigenvalues of some stability problems involving viscosity, J. Rat. Mech. Analysis **1**, No. 4, 579–603 (1952).

[14] H. Jeffreys and B. S. Jeffreys, Methods of mathematical physics (Cambridge, 1946).

[15] J. C. P. Miller, The Airy Integral, Mathematical tables, Part B, British Ass. for the Advancement of Science (Cambridge 1946).

[16] H. Weber, Zur Theorie der Besselschen Funktionen, Math. Ann. **37,** 404–416 (1890).

[17] G. N. Watson, Theory of Bessel functions, 2d ed. (Cambridge, 1948).

[18] Tables of the modified Hankel functions of order one third and of their derivatives (Computation Laboratory, Harvard University, Cambridge, Mass., 1945).

Los Angeles, November 20, 1952.

Journal of Research of the National Bureau of Standards Vol. 51, No. 4, October 1953 Research Paper 2452

Diffusion Length of Thermal Neutrons in Water

James A. DeJuren and Hyman Rosenwasser

The thermal-neutron diffusion length in a hydrogenous medium can be simply determined by measuring the variation of the thermal-neutron density at large radii from the center of a photoneutron source. The necessary requirement is that the relaxation length of the source in a medium be less than the diffusion length, so that diffusion dominates at large radii. Using a Ra-Be photoneutron source, the diffusion length of thermal neutrons was determined by indium-foil measurements at large radii. A value of 2.763 ± 0.015 cm was obtained. This result was confirmed in a second experiment with an Sb^{124}-Be source.

1. Introduction

In connection with the National Bureau of Standards program of absolute calibration of a standard-neutron source, the diffusion length of thermal neutrons in water was measured. A wide spread of values has been published, and the present experiment is compared with some of the earlier results.

For a high-energy neutron source the thermal-neutron density in water at large radii from the source decreases in accordance with the relaxation length defined below. If a source having only low-energy neutrons is employed so that the rate of neutron thermalization per unit volume falls off much more rapidly with increasing radius than the thermal-neutron density from a hypothetical thermal-point source, the thermal-neutron density at large radii will vary as a function of the diffusion length and radius only (as in the case of the thermal source). Photoneutron sources have sufficiently low maximum neutron energies for this purpose, and two sources having different neutron-energy maxima were selected for measurements. The general diffusion equation is

$$dn/dt = q - a + D\nabla^2 n, \tag{1}$$

where n is the thermal-neutron density, q is the rate of thermal-neutron production per unit volume (thermal-neutron source-strength density), and a is the absorption rate per unit volume.

$$a = nv/\lambda_a; \qquad D = \lambda_{tr} v/3,$$

where λ_a and λ_{tr} are the thermal-neutron absorption and transport mean free paths, respectively, for the average Maxwellian velocity, v, and D is the diffusion constant. The steady-state equation is

$$\nabla^2 n - n/L^2 + q/D = 0, \qquad \text{with } L^2 = \lambda_a \lambda_{tr}/3, \tag{2}$$

where L is the diffusion length. This equation has been amply treated by Fermi and others in standard texts.

With water as the medium and at large distances from the source, one can assume with sufficient accuracy that

$$q = Ke^{-r/b}/r^2, \tag{3}$$

where K is a constant, r is the distance from the source center, and b is the relaxation length.

This relation is very nearly obeyed even for a source with a broad spectral energy distribution such as is generated by Ra=Be(α,n). At large r, b is usually evaluated by measuring resonance activities at energies near thermal with Cd-covered foils. Then at large r

$$\nabla^2 n - \frac{n}{L^2} = \frac{K}{Dr^2} e^{-r/b}. \tag{4}$$

Since the distribution has spherical symmetry, let $n = u/r$. Then

$$\nabla^2 n = \frac{1}{r}\left(\frac{d^2u}{dr^2}\right)$$

and

$$\frac{d^2u}{dr^2} - \frac{u}{L^2} = \frac{K}{Dr} e^{-r/b}.$$

The solution to the equation satisfying the boundary condition $u \to 0$ as $r \to \infty$ is (derivation in appendix):

$$u = nr = \frac{KL}{2D} e^{-\frac{r}{L}} \left[C - \int_{\alpha_1 r}^{\infty} \frac{e^{-x}}{x} dx + e^{\frac{2r}{L}} \int_{\alpha_2 r}^{\infty} \frac{e^{-x}}{x} dx \right], \tag{5}$$

where $\alpha_1 = 1/b - 1/L$ and $\alpha_2 = 1/b + 1/L$. The exponential integrals $\int_{\alpha r}^{\infty} (e^{-x}/x)dx = EI(-\alpha r)$ may be evaluated from "Tables of sine, cosine and exponential integrals," NBS Mathematical Tables MT5 and 6 (U. S. Government Printing Office, Washington, D. C., 1947).

As $r \to \infty$, the solution may be expressed as

$$n = \frac{c_1 e^{-r/L}}{r} - \frac{b^2 L^2 k}{L^2 - b^2} e^{-r/b}. \tag{6}$$

If $L > b$, the first term will dominate at sufficiently large radii (the necessary requirement for evaluation of L).

Since the second term acts as a perturbation, measurements with sources having different values of b serve as a check on the effect of the perturbation at the radii where measurements are possible.

For a Ra-Be(γ,n) source the maximum neutron energy emitted is only 0.7 Mev (compared to 13 Mev

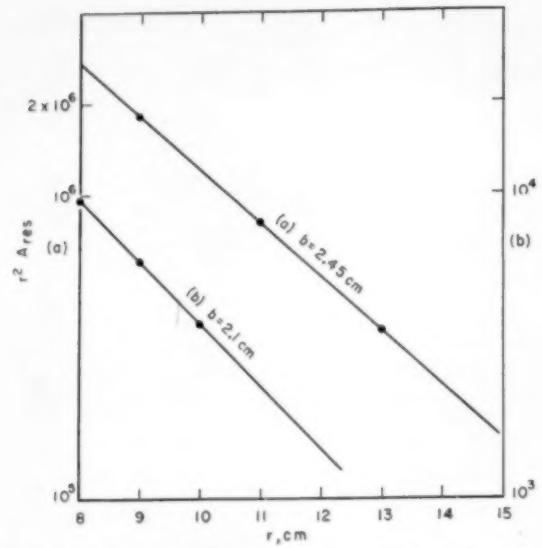

FIGURE 1. *Resonance data for the determination of the relaxation length.*

a, Ra-Be (γ,n) source, indium foils; b, Sb^{124}-Be source, gold foils.

for an α,n source), and the slowing-down length is short. Beyond 8 cm from the center of the National Bureau of Standards photoneutron standard [1][1] the indium resonance activity decreases in accordance with eq 3, with a relaxation length b=2.45 cm (fig. 1, a).

2. Experimental Arrangement

The Bureau photoneutron source was placed in the center of a 42-in. diameter stainless-steel tank filled with distilled water. Four indium foils, 2.0 by 3.4 cm^2 in area and 76 mg/cm^2 thick, held in light aluminum frames, were suspended by wires from a metal framework attached to the top of the tank. The foils were centered in the horizontal plane passing through the source at positions 90 deg apart. A cathetometer mounted horizontally above the tank made it possible to position the foils accurately to within a fraction of a millimeter at the radii employed. The source, a 4-cm-diameter Be sphere enclosing a 1-curie $RaBr_2$ capsule, was pin-mounted on a vertical stainless-steel rod extending from the tank floor.

Periodic measurements of the water temperature gave a mean value of 22° C, with maximum deviations of 2 deg.

3. Counting Techniques

The foils were activated to saturation at radii 14, 16, 18, 20, and 22 cm from the origin with and without 0.020-in. Cd covers. All four foils were simultaneously counted with "thin" mica end-window Geiger counters, the outputs of which were fed to a mixing circuit, which permitted the foils to be counted as a unit by a single scaler. The sides of the foils facing the source also faced the counter windows when placed in their respective holders inside the lead Geiger-counter shields. Uranium standards were used to monitor the Geiger counters, and repetitive cycles were made of standard, background, and foils, with counting intervals of 5, 10, and 20 minutes, respectively, during the decay of the foils.

[1] Figures in brackets indicate the literature references at the end of this paper.

4. Results

The data are given in table 1. A correction of 6 percent must be made for the absorption of 1.44 ev In resonance neutrons by the Cd covers. Errors given are determined by the consistency of the data as well as the counting statistics. The activities given are the counting rates of the foils at saturation normalized to the same monitor reading. Figure 2 is a semilog plot of radius times thermal activity as a

TABLE 1. *Data from NBS standard* Ra-Be *photoneutron source*

Position (r in cm)	Activity without Cd (Counts per minute)	Resonance activity × 1.06 (Counts per minute)	Thermal activity (A_{th}) (Counts per minute)	rA_{th}
14.0	7,657 ±38	190 ±7	7,467 ±39	104,540
16.0	3,546 ±18	64 ±15	3,482 ±23	55,710
18.0	1,533 ±9	[a]22 ±6	1,511 ±11	27,200
20.0	655 ±10	[a]8 ±3	647 ±10	12,940
22.0	292 ±5	[a]3 ±1	289 ±5	6,360

[a] Calculated.

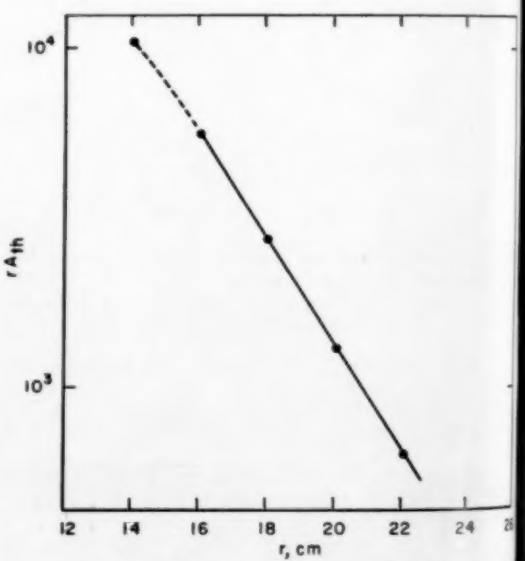

FIGURE 2. *Indium foils in water.*

Ra-Be (γ,n) source.

function of r. Beyond 16 cm, rA_{In} decreases exponentially.

$$\frac{A_1 r_1}{A_2 r_2}(1\pm\epsilon)=e^{\frac{r_2-r_1}{L}},$$

where ϵ is the experimental error of the ratio

$$\ln\left(\frac{A_1 r_1}{A_2 r_2}\right)\pm\epsilon=\frac{r_2-r_1}{L}.$$

Using the data at 16 and 22 cm as an example,

$$\ln\frac{5571}{636}\pm\epsilon=\frac{6}{L}$$

$$2.170\left(1\pm\frac{\epsilon}{2.170}\right)=\frac{6}{L};\quad \epsilon=0.018$$

$$L=2.765\pm0.023 \text{ cm}.$$

The weighted least-squares fit of the data between 16 and 22 cm yield $L=2.763\pm0.015$ cm.

5. Sb^{124}-Be Experiment

An antimony pellet that was irradiated in the Oak Ridge National Laboratory pile for 2 months was substituted for the $RaBr_2$ capsule in a 4-cm-diameter beryllium sphere. The 60-day Sb^{124} has three γ-rays above the Be photoneutron threshold, the principal one having an energy of 1.7 Mev and giving rise to 24-kev neutrons [2]. As the neutron energies are considerably lower than those from the NBS standard source, moderation occurs closer to the source, and the relaxation length is shorter. A value of 2.1 cm for b was obtained from the Sb-Be source in water, the measurements being made with Cd-covered indium and gold foils at radii beyond 8 cm from the source (fig. 1,b).

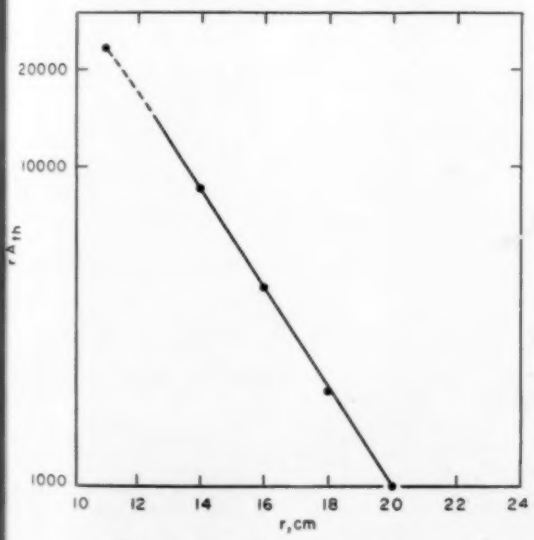

FIGURE 3. *Indium foils in water.*
Sb^{124}-Be source.

TABLE 2. *Data from* Sb^{124}-Be *photoneutron source*

Position (r in cm)	Activity without Cd (Counts per minute)	Resonance activity × 1.06 (Counts per minute)	Thermal activity (A_{th}) (Counts per minute)	rA_{th}
14.0	625.8 ±6	12.4 ±3.0	613.4 ±7	8,588
16.0	262.3 ±10	[a] 1.5 ±0.5	260.8 ±10	4,173
18.0	110.7 ±6	[a] 0.5 ±0.2	110.2 ±6	1,984
20.0	50.6 ±5	[a] .2 ±0.1	50.4 ±5	1,008

[a] Calculated.

Indium foils that had been intercalibrated in the same slow neutron flux were simultaneously exposed to saturation at different radii from the source. The foils were successively removed and counted with the same end-window tube. For radii greater than 12 cm, rA_{In} decreases exponentially. At 14 cm the corrected cadmium reading is 1 percent of the thermal reading and decreases to 0.35 percent at 20 cm (calculated by using $b=2.1$). The least-squares fit of the data (table 2) gives a value of L equal to 2.76 ±0.07 (fig. 3), which is in agreement with the Ra-Be result, even though the ratio of indium resonance to thermal-neutron counting rates is considerably lower for the Sb-Be over the range covered.

6. Discussion and Comparison of Results

For a purely thermal source located at the origin

$$n(r)=Ce^{-r/L}/r$$

and

$$\overline{r^2}=\frac{\int_0^\infty n(r)\,r^4dr}{\int_0^\infty n(r)\,r^2dr}=6L^2.$$

In analogy, the slowing-down distance, L_s, of neutrons from a high-energy source is usually estimated from the mean-square distance obtained from resonance-neutron measurements. $\overline{r^2}_{res.}=6L_s^2$, and the approximate relation

$$\overline{r^2}_{thermal}=\overline{r^2}_{res.}+6L^2 \tag{7}$$

is used to calculate L^2.

Equation (7) treats the resultant thermal-neutron distribution as though the high-energy neutrons diffused from the source with a diffusion length equal to $\sqrt{L_s^2+L^2}$. The shape of the radial thermal and resonance-neutron density distributions are actually Gaussian near the origin. As a result, the thermal and resonance $\overline{r^2}$ values give somewhat overestimated diffusion lengths, and the value of L obtained by this method should represent an upper bound to the true figure.

Table 3 lists some of the early values obtained with RaBe(α,n) sources, using eq 7.

TABLE 3.

Detector	$\overline{r^2}_{thermal}$	$\overline{r^2}_{res.}$	L	b	L_0
	cm^2	cm^2	cm	cm	cm
Rh [3]	327	277	2.85	9.4	6.8
In [4]	337	272	3.3	9.4	6.7
Dy+In [5]	330	278	2.94	10.1	6.8
In [6]	371	288	3.6	9.4	6.9
In [7]	363	313	2.88	9.8	7.2

Since eq 7 involves a small difference between two numbers, a 1 percent error in either $\overline{r^2}$ term causes about a 3-percent error in L.

Berthelot, Cohen, and Reel [8] have determined L with a Ra-Be(α,n) source in a water tank by a different technique. A thin spherical shell, which could be filled alternately with H_2O (or $H_2O+H_2SO_4$) and a $CdSO_4$ solution, surrounded the source. The difference in the neutron densities outside the sphere for the two cases arises from the diffusion of thermal neutrons present when the sphere is filled with water. Measurements with foils gave a best value of 2.77 ± 0.04 cm for the thermal-diffusion length.

Larsson [9] recently has made extensive measurements of the same type at different $CdSO_4$ concentrations. An attempt was made to correct for the perturbation in the slow-neutron density in the immediate vicinity of the sphere and for the attenuation of high-energy neutrons by the cadmium. He obtained a diffusion length of 3.25 ± 0.13 cm. However, a different interpretation of the data would give a lower value.

Perhaps the simplest method for measuring L is afforded by a nuclear reactor. If a water tank is placed on top of a thermal column, the neutron density, a few transport mean free paths from the boundary should decrease as $e^{-z/L}$, providing that the diameter and height of the tank are much greater than the diffusion length. Early reactor experiments gave a value of about 2.8 cm. Sisk [10] has recently obtained a value of 2.67 ± 0.02 cm at 24° C, using the Oak Ridge pile and different boundary conditions.

Probably most of the variation in the values of L obtained by the different techniques is due to the failure to meet experimentally the rigorous boundary conditions required.

In the present experiment an upper limit to L is obtained unless the bracketed term in eq 5 can be determined. The exponential integrals have been evaluated, using $L=2.76$, and C was roughly determined for the radium source by calibrating the foils in a standard flux. A perturbation of less than 5 percent ($C>1.3$) in L should be caused by neglecting the exponential integrals. For the Sb-Be source, the exponential integrals are much smaller, and neglecting them should affect the calculation of L less. The Sb-Be(γ,n) source was fairly weak, and a stronger source would permit measurements beyond 20 cm, where the exponential integrals would have negligible effect.

The advice and cooperation of L. F. Curtiss is gratefully acknowledged, as well as the assistance of R. N. Olcott, D. Padgett, and W. Bailey in obtaining the experimental data of this paper. We are indebted to A. N. Gleyzal for assistance in the solution of the diffusion equation.

7. References

[1] L. F. Curtiss and A. Carson, Phys. Rev. **76,** 1412 (1949).
[2] K. Way, Nuclear Data, NBS Circular 499 (1950).
[3] E. Amaldi and E. Fermi, Phys. Rev. **50,** 899 (1936).
[4] J. H. Rush, Phys. Rev. **73,** 271 (1948).
[5] Munn and Pontecorvo, Can. J. Research **25A,** 157 (1947).
[6] C. W. Tittle, MIT Ph. D. Thesis, January 1948.
[7] J. Dacey, R. Paine, and C. Goodman, unpublished report.
[8] Berthelot, Cohen and Reel, Compt. rend. **225,** 406 (1947).
[9] Larsson, Arkiv. Fysik, **2,** 47 (1950).
[10] F. J. Sisk, Oak Ridge National Laboratory Report 933 (1951).

8. Appendix

Solution of diffusion equation:

$$\frac{d^2u}{dr^2}-\frac{u}{L^2}=-\frac{K}{Dr}e^{-r/b}.$$

Let $p=\frac{\partial}{\partial r}$

$$(p-1/L)(p+1/L)u=-\frac{K}{Dr}e^{-r/b}$$

$$u=\frac{-1}{(p-1/L)(p+1/L)}\frac{K}{Dr}e^{-r/b}.$$

Solving by partial fractions:

$$\frac{1}{(p-1/L)(p+1/L)}=\frac{S_1}{p-1/L}+\frac{S_2}{p+1/L}$$

$$S_1=L/2, \qquad S_2=-L/2$$

$$u=LK/2D\left[\frac{1}{p+1/L}-\frac{1}{p-1/L}\right]\frac{e^{-r/b}}{r}$$

$$u=C_1e^{-r/L}+C_2e^{+r/L}+KL/2D$$
$$\left[e^{-r/L}\int\frac{e^{-r(1/b-1/L)}}{r}\,dr-e^{r/L}\int\frac{e^{-r(1/b+1/L)}}{r}\,dr\right].$$

Let $\alpha_1=1/b-1/L$, $\alpha_2=1/b+1/L$.

The indefinite integrals may be expressed in terms of definite exponential integrals

$$\int\frac{e^{-\alpha r}}{r}\,dr=-\int_r^\infty\frac{e^{-\alpha y}}{y}\,dy=-\int_{\alpha r}^\infty\frac{e^{-x}}{x}\,dx.$$

To satisfy boundary conditions at infinity $C_2=0$, and setting $C_1=KLC/2D$.

$$u=nr=\frac{KL}{2D}e^{-r/L}\left[C-\int_{\alpha_1 r}^\infty\frac{e^{-x}}{x}\,dx+e^{2r/L}\int_{\alpha_2 r}^\infty\frac{e^{-x}}{x}\,dx\right]$$

To evaluate C, K must be determined. Since less than 1 percent of the neutrons from either source are captured above thermal energies

$$Q=4\pi\int_{r_0}^\infty q(r)r^2dr=4\pi\int_{r_0}^\infty -Ke^{-r/b}dr,$$

where Q is the neutron emission rate of the source.

$$Q=4\pi bKe^{-r_0/b}.$$

The expression $q=Ke^{-r/b}/r^2$ does not hold down to the radius of the source, so a larger value of r_0 than the source radius must be used. For the Ra-Be(γ,n) source r_0 is estimated to be between 4.0 and 4.5 cm from previous data. Using $K=Qe^{r_0/b}/4\pi b$, an absolute measurement of n would permit a rough determination of C as all other quantities are approximately known.

Exponential integrals for $L=2.76$:

Source	α_1	α_2
Ra-Be	0.0458	0.7705
Sb-Be	.114	.8385

r	$\int_{\alpha_1 r}^{\infty} e^{-x}/x\,dx$	$e^{2r/L}\int_{\alpha_2 r}^{\infty} e^{-x}/x\,dx$
	Ra-Be(γ,n) source	
cm		
16	0.351	0.037
18	.297	.030
20	.253	.024
22	.217	.019
	Sb-Be(γ,n) source	
14	0.0868	0.0161
16	.0625	.0113
18	.0455	.0078
20	.0339	.0054

WASHINGTON, July 1, 1953.

U. S. GOVERNMENT PRINTING OFFICE: 1953

UNITED STATES
GOVERNMENT PRINTING OFFICE
DIVISION OF PUBLIC DOCUMENTS
WASHINGTON 25, D. C.

OFFICIAL BUSINESS

PENALTY FOR PRIVATE USE TO AVOID PAYMENT OF POSTAGE, $300 (GPO)

Journal of Research of the National Bureau of Standards Vol. 51, No. 4 October 1953

Contents

		Page
Determination of carbon 14 in the terminal positions of sugars: Preparation of D-arabinose-5-C^{14} from D-fructose-1,6-C^{14}. Harriet L. Frush and Horace S. Isbell.	RP2446	167
Measurement of variations in atmospheric refractive index with an airborne microwave refractometer. Howard E. Bussey and George Birnbaum.	RP2447	171
Studies in the system magnesia-silica-water at elevated temperatures and pressures. Elmer T. Carlson, Richard B. Peppler, and Lansing S. Wells.	RP2448	179
Dielectric properties of Teflon from room temperature to 314° C and from frequencies of 10^2 to 10^5 c/s. Paul Ehrlich.	RP2449	185
pH of solutions of potassium tetroxalate from 0° to 60° C. Vincent E. Bower, Roger G. Bates, and Edgar Smith.	RP2450	189
On small disturbances of plane Couette flow. Wolfgang Wasow.	RP2451	195
Diffusion length of thermal neutrons in water. James A. DeJuren and Hyman Rosenwasser.	RP2452	203

Single copies of the above Research Papers are not available for sale, but the Superintendent of Documents, U. S. Government Printing Office, Washington 25, D. C., will reprint 100 or more copies, and request for the purchase price should be mailed promptly to that Office.

For sale by the Superintendent of Documents, U. S. Government Printing Office, Washington 25, D.C. Price 30 cents (single copy). Subscription Price: $5.50 a year; $1.25 additional for foreign mailing. Single copies vary in price.

UNITED STATES GOVERNMENT PRINTING OFFICE, WASHINGTON : 1953